# Strange metal to insulator transitions in the lowest Landau level

Ben Currie [*] and Evgeny Kozik

*Department of Physics, King's College London, Strand, London WC2R 2LS, United Kingdom*

We study the microscopic model of electrons in the partially-filled lowest Landau level interacting via the Coulomb potential by the diagrammatic theory within the *GW* approximation. In a wide range of filling fractions and temperatures, we find a homogeneous non-Fermi liquid (nFL) state similar to that found in the Sachdev-Ye-Kitaev (SYK) model, with logarithmic corrections to the anomalous dimension. In addition, the phase diagram is qualitatively similar to that of SYK: a first-order transition terminating at a critical end-point separates the nFL phase from a band insulator that corresponds to the fully filled Landau level. This critical point, as well as that of the SYK model—whose critical exponents we determine more precisely—are shown to both belong to the Van der Waals universality class. The possibility of a charge density wave (CDW) instability is also investigated, and we find the homogeneous nFL state to extend down to the ground state for fillings $0.2 \lesssim \nu \lesssim 0.8$, while a CDW appears outside this range of fillings at sufficiently low temperatures. Our results suggest that the SYK-like nFL state should be a generic feature of the partially filled lowest Landau level at intermediate temperatures.

## I. INTRODUCTION

Two-dimensional electrons subject to strong magnetic fields exhibit an extreme variety of highly correlated quantum phases. Key examples are the fractional quantum Hall (FQH) states [1,2], whose strong correlations are manifest in the emergence of low-energy quasiparticles possessing fractional charge and statistics [3,4], which arise due to strong Coulomb interactions within a flat band. Being an inherently nonperturbative phenomenon, the development of a microscopic theory of the FQH states—based solely on the electronic degrees of freedom and their Coulomb interactions—remains an important open problem. An understanding has been achieved using trial wave functions [5,6] and effective field theories of emergent fermions—such as composite fermions (CFs) [6–11]. At mean-field level, the CFs, which are bound states of electrons and an even number of flux quanta, move in a partially canceled magnetic field, resulting in insulating behavior at odd-denominator filling fractions and metallic properties at even denominators. While the existence of emergent fermions that experience a weaker magnetic field has been confirmed spectacularly by experiments at low temperatures [12–18], the nature of the state of the system at higher temperatures remains unknown.

Owing to the strong coupling nature of the problem, controlled solutions of the electronic Hamiltonian have been limited to exact diagonalization [19–25] and DMRG calculations [26–32] at finite system size. These methods allow exact calculation of the ground and excited state properties, but are limited to small system sizes. In the thermodynamic limit, no method has yielded results consistent with experiment. Hartree-Fock calculations were performed early-on [33–35] and yielded charge density wave (CDW) states for all filling fractions. In addition, using the (partially self-consistent) *GW* approximation, Tao and Thouless considered a periodic occupation of the lowest Landau level single-particle wave functions and found the existence of a gap to all excitations at all integer-denominator filling fractions $\nu = \frac{1}{m}$ [36,37]. A fully self-consistent homogeneous solution of the *GW* equations was obtained by Haussmann [38] in an effort to understand the nature of the pseudogap in the single-electron density of states observed in experiments [39–44]. Since a metallic state was observed instead, its physical implications and relevance to the lowest Landau level physics as well as related models was not realized.

In this paper, we revisit the *GW* theory for this problem and analyze it in full detail without further approximations. We obtain the phase diagram in the full space of parameters, which reveals two distinct types of metal-to-insulator transition. We pay particular attention to the metallic non-Fermi liquid (nFL) state found in a wide range of parameters at intermediate temperatures, as well as the critical point of its transition to a fully filled Landau level band insulator. As a byproduct, we reconcile the different diagrammatic results, and discuss the shortcomings and successes of each.

We start from the microscopic model of electrons in the lowest Landau level (LLL) interacting via the long-range Coulomb potential in the thermodynamic limit. At partial-filling of the LLL, the noninteracting limit yields a macroscopically degenerate ground state, thus rendering an approach based on an expansion around it very challenging. The lowest-order terms, corresponding to the mean-field (Hartree-Fock) theory, have been understood for some time [33–35], and yield CDW band insulator ground

---

*Corresponding author: benjamin.currie@kcl.ac.uk

states for all filling fractions. This, however, contradicts the experimental observation that FQH states possess no long-range order [45]. Moreover, the expansion in the bare interaction cannot be properly justified in the thermodynamic limit since terms beyond first-order are divergent due to the long range of the Coulomb interaction. For this reason, an expansion in the screened interaction is necessary. We access nonperturbative physics by formulating a diagrammatic series that is renormalized self-consistently to infinite order in both the one-electron ($G$) and screened Coulomb interaction ($W$) channels. In this study, the diagrammatic expansion is truncated at the level of the $GW$ approximation, in which the electronic self-energy $\Sigma$ is given by the $GW$ diagram and the polarization $\Pi$ renormalizes the interaction by $GG$ [46]. We note that our approach is the same as that used by Hauss-mann [38], but differs from the approach of Tao and Thouless, which uses only partial self-consistency. Importantly, we find that the Tao Thouless states are in fact not (fully) self-consistent solutions of the $GW$ equations (this point will be further discussed in Sec. III). We envisage that this theory will be systematically extended to sufficiently higher orders in the future by means of advanced diagrammatic Monte Carlo techniques [47–51], which could enable *a priori* control of the potential systematic error. Our $GW$ results, however, are a necessary starting point for such extensions. Most importantly, being controlled in the high temperature limit, they already suggest a nontrivial and rich physical picture of the LLL at finite temperatures.

In particular, we demonstrate that the CDW physics obtained at the mean-field level is altered fundamentally: there is no continuous transition to density-wave ordering down to (and including, at the $GW$ level) $T = 0$ for $0.2 \lesssim \nu \lesssim 0.8$, and the resulting metallic state is an nFL of the type described by the prototypical Sachdev-Ye-Kitaev (SYK) model [52–54]—a model with random all-to-all $q$-fermion coupling, denoted $SYK_q$ (with $q = 4$ in the original case). Specifically, this nFL phase displays quantum criticality, characterized by a power-law low-frequency scaling of the fermion self-energy,

$$\Sigma(i\omega) = \lambda e^{-i\text{sign}(\omega)(\pi/2+\theta)}|\omega|^{1-2\Delta}, \text{ for } \omega \to 0, \quad (1)$$

with the so-called anomalous dimension $0 < \Delta < 1/2$, constant $\lambda > 0$, and particle-hole asymmetry parameter $\theta$, which controls the filling fraction of the LLL and which must satisfy $-\pi\Delta < \theta < \pi\Delta$. A solution of this form is relevant to the normal state of high temperature superconductors [55–57] and is closely related to extremal black-holes due to the emergent low-energy conformal symmetry and the saturation of the chaos bound on the Lyapunov exponent [58–60]. Physically, it describes a compressible metal without coherent electronic quasiparticle excitations. In certain SYK-inspired models in nonzero spatial dimension, it is known that Eq. (1) leads to linear-in-temperature resistivity [61–64], which is the main signature of the ubiquitous strange metal phase [65–67].

Our nFL solution is described by Eq. (1) with $\Delta = \frac{1}{4}$ in the theoretical limit $\omega \to 0$; however, at any practically relevant frequency, the long-range nature of the Coulomb interaction gives rise to appreciable logarithmic corrections to $\Delta$. This state is found in a broad range of filling fractions centered around one-half, as summarized in the phase diagram in
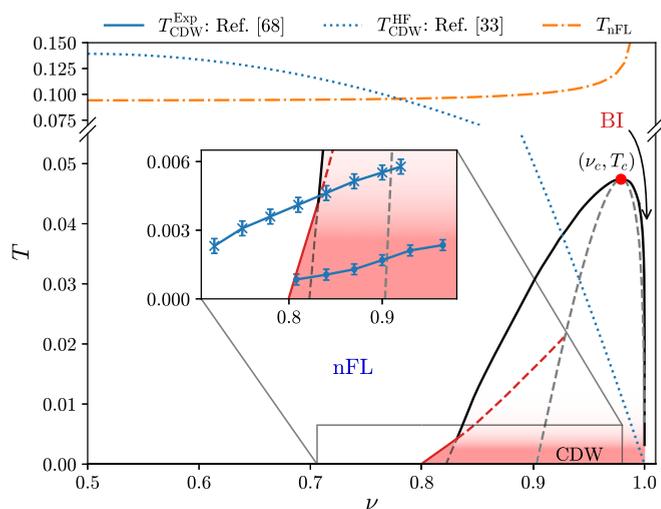


FIG. 1. Phase diagram of the model (3) within the $GW$ approximation in the temperature ($T$, in units of $e^2/\ell_B$ which at typical magnetic fields $B = 13$ T corresponds to $\sim$200 K) against filling fraction ($\nu$) plane. The non-Fermi liquid (nFL) phase of quantum-critical fermions exists down to low $T$ and for a broad range of $\nu$, and below the free fermion thermal state to nFL crossover temperature $T_{\text{nFL}}$ (orange dash-dot line). At some transition filling $\nu_{\text{nFL-BI}}(T)$, the nFL undergoes a first-order transition to a band-insulating (BI) phase corresponding to the fully filled LLL (solid black line). Phase separation occurs inside this region, in which the nFL and BI phases coexist, while metastable phases exist between the solid black and grey dashed lines. The second-order critical point of this transition is labeled by $(\nu_c, T_c)$ (red point). In addition, a second-order charge-density wave (CDW) transition is observed from the nFL phase at low temperatures $T_{\text{CDW}}(\nu)$ (red line). Inside the phase-separation region, the location of the CDW transition is unknown, and the boundary of the CDW phase is indicated by the blurring. The metastable nFL phase undergoes a CDW transition shown by the red dashed line. Experimental CDW transition temperatures reported in Ref. [68] are shown for both heterojunction (dots) and quantum well (crosses) samples. Also shown is the Hartree-Fock charge-density-wave temperature $T_{\text{CDW}}^{\text{HF}}$ obtained in Ref. [33].

Fig. 1, and emerges from the high-temperature (free fermion) thermal state at the crossover temperature $T_{\text{nFL}} \sim 0.1\, e^2/\ell_B$. Similarly to the SYK model [69,70], as the filling fraction is increased at low temperatures, the nFL state undergoes a first-order transition to a fully filled-LLL band insulator, with the transition line ending at a critical point $(\nu_c, T_c)$ (see Fig. 1).

We study the critical point specifically, calculating the critical exponents and comparing them to those in the SYK model. To this end, we reconsider the critical point of the $SYK_4$ model, and demonstrate that the corresponding critical exponents actually differ from those reported previously [69,70]. Instead, the values we obtain for $SYK_4$ agree with those found recently in the $q \to \infty$ limit in Ref. [71]. Remarkably, we find precisely the same exponents for the LLL model, indicating that the critical points of the LLL and the $SYK_q$ models for all $q$ belong to the same universality class: the Van der Waals universality class, also describing an extremal black hole. This answers in the affirmative the question raised in Ref. [71] of whether the critical points of the $SYK_4$ and $SYK_{q=\infty}$ models are the same.

Compared to the SYK model, the phase diagram is enriched by the presence of the CDW insulating state. Experimentally, CDW phases are known to exist only for extremal Landau level filling fractions $\nu \lesssim 0.25$ and $\nu \gtrsim 0.75$ [72–77], and our results predict a CDW ground state in qualitative agreement with these observations (the $\nu \lesssim 0.25$ range is a mirror image of $\nu \gtrsim 0.75$ due to the particle-hole symmetry). At larger filling fractions close to the nFL-to-band insulator transition and at low temperature, we find that the transition to the CDW phase is continuous. In addition, the corresponding critical temperatures $T_{CDW}(\nu)$ are the same order of magnitude as those observed in experiments performed on GaAs/AlGaAs heterojunctions and AlGaAs/GaAs/AlGaAs quantum wells [68,77,78] (data from Ref. [68] are shown in Fig. 1 for both types of sample).

Although the *GW* approximation is controlled in the high temperature limit, the observed nFL state exists only at low temperatures, for which the higher-order terms cannot be neglected *a priori*. Nonetheless, additional observations allow us to suggest that the nFL physics predicted by *GW* should indeed describe the normal phase from which the fractional quantum Hall states emerge as the temperature is lowered. Specifically, the *GW* results are in qualitative agreement with the exact results in the thin-torus (TT) limit, in which the ground states are the Tao-Thouless states [79–82]. We find that the low-temperature *GW* solution in this limit is indeed a TT state, while at intermediate temperatures it transforms to a nFL phase that is qualitatively similar to that observed in the thermodynamic limit. Thus, since *GW* gives correct physics both in the limit of high temperatures and in the TT limit at low temperatures, by continuity we expect that it captures the physics in the thermodynamic limit at some intermediate temperatures as well, where the nFL state is predicted.

Our finding of the nFL at intermediate temperatures within the LLL is also consistent with empirical evidence from other systems where interactions completely dominate the kinetic energy. One example is the twisted bilayer graphene near the magic angle, in which nFL quantum critical states have been found experimentally [83–85]. There, the normal state preceding the low-temperature fractionally filled insulator is also an nFL state [83,86,87]. In addition, it has been proposed [88,89] that a graphene flake subject to a strong perpendicular magnetic field could serve as an experimental realization of SYK physics, due to the absence of any dispersion and the spatial randomness of the interaction stemming from the irregular shape of the boundary. More generally, it is known that the generic class of Hamiltonians which conserve both center of mass momentum *and* center of mass position cannot possess gapless ground states that are ordinary metals (here defined as phases which possess a nonzero Drude weight) [90]. Since the LLL Hamiltonian belongs to this class, any metallic state must be an nFL in nature. Experimental work on the high temperature properties of the partially filled LLL, which is currently lacking, would be crucial to verify our predictions experimentally.

This paper is organized as follows. In Sec. II, we derive the microscopic Hamiltonian and discuss the single-particle physics. In Sec. III, we present the diagrammatic formulation of this problem and the *GW* approximation. In Sec. IV, we consider translationally symmetric solutions of the *GW*

equations. The nFL solution is discussed in detail, as well as the phase diagram displaying the nFL to band insulator transition. The corresponding critical point is also analysed, with particular focus on calculation of the critical exponents. In Sec. V, continuous phase transitions to density wave ordered solutions are discussed. Finally, we put the *GW* results in a broader context and discuss their relevance to the LLL physics in Sec. VI.

## II. MODEL

The two-dimensional electron system is subject to a large homogeneous and perpendicular magnetic field $B = (0, 0, -B)$. The strong magnetic field implies that the electrons are spin polarized and thus only one spin component is considered. We work in Landau gauge, in which the vector potential is $A = (0, -Bx, 0)$. This choice of gauge explicitly breaks the translation invariance in the $x$ direction. Since, however, the $y$-translation symmetry is preserved, the $y$ component of momentum $k$ is a good quantum number and can be used to label the single-particle states.

The lowest Landau level (LLL) eigenfunctions are

$$\psi_k = \frac{1}{\sqrt{\ell_B \sqrt{\pi}}} e^{iky} e^{-\frac{1}{2\ell_B^2}(x - k\ell_B^2)^2}, \tag{2}$$

where $\ell_B = \sqrt{\frac{\hbar}{eB}}$ is the magnetic length, $k = 2\pi n/L_y$, and $L_x$ and $L_y$ are the system sizes in the $x$ and $y$ direction. Notably, the wave functions are localized in the $x$ direction at the position $x = k\ell_B^2$, with localization width $\ell_B$. This is a manifestation of the explicitly broken $x$-translation symmetry in Landau gauge. The corresponding eigenenergies are independent of $k$ and are equal to $E = \hbar\omega_B/2$ with $\omega_B = eB/m$ the cyclotron frequency. Therefore the LLL contains a macroscopic number of states $D = \frac{L_x L_y}{2\pi \ell_B^2}$, all of which are degenerate. The higher Landau levels are separated from the LLL by a gap $\propto B$, which allows us to ignore them entirely. In the following we set $E = 0$, and consider the thermodynamic limit $L_x, L_y \to \infty$, in which the momentum $k$ is continuous.

In the basis of single-electron states (2), the Hamiltonian in terms of the corresponding creation ($c_k^\dagger$) and annihilation ($c_k$) operators is

$$H_1 = \frac{1}{2} \sum_m \sum_{kq} V_{kqm} c_{m+q}^\dagger c_{m+k}^\dagger c_{m+q+k} c_m - \sum_m \mu c_m^\dagger c_m, \tag{3}$$

where the momentum summations are a shorthand for $\sum_k = \int \frac{dk}{2\pi}$ (we use this notation throughout), and

$$V_{kqm} \equiv V_{kq} = \int \frac{dp}{2\pi} \frac{2\pi}{\sqrt{p^2 + q^2}} e^{-\frac{1}{2}(p^2 + q^2)\ell_B^2} e^{ipk\ell_B^2} \tag{4}$$

is the Coulomb potential $V(r) = \frac{1}{r}$ projected onto the LLL and represented diagrammatically as

$$V_{kqm} = \qquad . \tag{5}$$

In the following, we use units in which $\ell_B = 1$, and measure all energies in units of $e^2/\ell_B$.

In realistic systems, a uniform positive background charge density is required to ensure charge-neutrality and hence thermodynamic stability. In two dimensions and in a nonzero external magnetic field, the stability of interacting electrons is very fragile because of the large exchange energy, which can lead to negative compressibility $\kappa$ [91–94]. In the inversion-layer materials used in experiments, the two-dimensional plane in which the electrons reside is located at the interface between two semiconductors with differing band-gaps, and the plane of positive background charge (here the donor ions) is separated from this electron plane by a small distance $d$ [95]. While the $d = 0$ case leads to $\kappa < 0$ for generic densities, nonzero $d$ introduces a positive capacitance energy, which can offset and nullify the (negative) exchange energy for large enough separation $d$. This ensures $\kappa > 0$ for all electron densities. In this paper, for simplicity, we consider a separation such that the (homogeneous) exchange term is canceled exactly, which allows us to simply set the spatially uniform components of this term to zero. We note that while dynamical properties of the nFL phase are unchanged by the value of $d$, the thermodynamic properties—for example, the compressibility—are altered. Therefore the parameters at which phase transitions occur at nonzero $d$ will in general differ from those reported here at $d = 0$.

### III. DIAGRAMMATIC FORMULATION AND *GW* APPROXIMATION

Our main observable, containing the information about the state of the system and its excitation properties, is the finite-temperature (Matsubara) Green's function of the electrons in the LLL, which is defined as [96]

$$G_k(\tau) = -\langle \mathcal{T} c_k(\tau) c_k(0)^\dagger \rangle, \tag{6}$$

where $\mathcal{T}$ is the time-ordering operator for the imaginary time $\tau$. It can be obtained through a calculation of the electronic self-energy $\Sigma$, which contains the combined effect of electron interactions on one-particle excitations, via the Dyson equation [96]

$$G_k(i\omega) = \frac{1}{i\omega + \mu - \Sigma_k(i\omega)}, \tag{7}$$

where $\omega$ is the Matsubara frequency. In the diagrammatic theory, $\Sigma$ is formulated as an expansion in the powers of the coupling vertex, with each term represented graphically by the corresponding number of vertices (5) connected by the Green's functions and integrated over all internal variables. In particular, the first-order self-energy diagrams yield

$$\Sigma_k(i\omega) = \frac{1}{\beta} \sum_\nu \int \frac{dq}{2\pi} (V_{q,0} - V_{0,q}) G_{k-q}(i\omega - i\nu), \tag{8}$$

where the first and second terms correspond to the Hartree and Fock contributions of the mean-field theory, respectively. In the homogeneous high-temperature phase, the Hartree-Fock self-energy is a trivial (i.e., momentum and frequency independent) energy shift. However, as discussed in the introduction, it develops an instability towards CDW order at

intermediate temperatures $T_{\mathrm{CDW}}^{\mathrm{HF}} \sim 0.1 e^2/\ell_B$ for all LLL fillings (blue dotted curve in Fig. 1: see Appendix A for more details). Since the first order gives no new physics in the homogeneous phase, which is of primary interest to us here, we now move on to higher-order.

Systematically going beyond the mean-field by including higher order in $V$ terms is plagued by Dyson's collapse [97] in the LLL model as at $B = 0$, which renders the expansion in the bare $V$ divergent with zero convergence radius. There are currently a number of ways to address the problem, such as, e.g., by an arbitrary dressing of the interaction with the explicit inclusion of the corresponding counter-terms in the expansion [50,98,99], or by a more general homotopy of the microscopic model [100]. Both methods, however, are only supposed to yield physically meaningful results at sufficiently high orders of the expansion. We thus adopt the standard approach of reformulating the expansion in terms of the interaction $W$ that is self-consistently screened by the electron polarization $\Pi$ [46]:

$$W_{k_1,k_2;q}(i\nu) = V_{(k_1-k_2)q} + \sum_{k_3} V_{(k_1-k_3)q}\,\Pi_{k_3;q}(i\nu)\,W_{k_3,k_2;q}(i\nu), \tag{9}$$

where $\omega$ and $\nu$ are fermionic and bosonic Matsubara frequencies, respectively. Here, the self-energy $\Sigma$ and polarization $\Pi$ are irreducible (skeleton) expansions in terms of $G$ and $W$ which themselves are to be computed self-consistently [46,96]. This formulation is formally exact and could in principle be evaluated to high expansion orders by bold-line DiagMC techniques [47–49,101,102] to yield results with controlled error bars. However, the DiagMC approach with self-consistency in two channels poses substantial technical challenges and typically builds upon an accurate deterministic solution of the problem at the lowest order of the diagrammatic expansion [49], which we derive here. This is the so-called self-consistent *GW* approximation, where

$$\Sigma_k(i\omega) = -\frac{1}{\beta} \sum_{i\nu} \int \frac{dq}{2\pi} W_{k-q,k-q;q}(i\nu) G_{k-q}(i\omega - i\nu) \tag{10}$$

and

$$\Pi_{k_3;q}(i\nu) = \frac{1}{\beta} \sum_{i\omega} G_{k_3+q}(i\omega + i\nu) G_{k_3}(i\omega). \tag{11}$$

Equations (7), (9) (10), and (11) form a closed set, which we solve here by iterations without any additional approximations. For this we utilize the discrete Lehmann representation [103], which enables compact representation of the frequency dependence of all quantities.

While the truncation to *GW* is uncontrolled in general, it can be shown that at high temperature, the *GW* diagram is leading order in $T$. This is a consequence of the long-range nature of the Coulomb interaction, and is similar to the dominance of the same diagrams in the zero magnetic field electron gas [104]. The same is true for large $\mu$, and hence also for large (and small) filling fractions.

Tao and Thouless solved the *GW* equations at zero temperature, by approximating the self-energy to be frequency independent [36,37]. This is similar to the quasiparticle self-consistent *GW* approximation [105–107]. The resulting states, named TT states, were found to have microscopic (in the sense

that their wavelength $\lambda \ll \ell_B$) periodic modulations of the charge density, and a charge gap for all fractional fillings, including those with even denominators. Details of the TT approach, and the related thin-torus limit in which the TT states are the exact ground states, are given in Appendix B. We find, however, that including the full dynamics due to the frequency dependence destroys the TT states in the thermodynamic limit, as shown below.

## IV. HOMOGENEOUS SOLUTION

In this section, we confine ourselves to the generic case of transitionally symmetric solutions and consider the possibility of breaking this symmetry separately in the next section. Due to our choice of the gauge, the $y$ component of the momentum $k$ plays an unusual role. The lack of the translational invariance in the $x$ direction implies that the system becomes inhomogeneous whenever $G$ features a nontrivial dependence on $k$. This can be seen by considering the density operator in the momentum space

$$\rho(\mathbf{q}) = \int d^2 r \, e^{-i\mathbf{q}\cdot\mathbf{r}} \phi^\dagger(\mathbf{r}) \phi(\mathbf{r}), \qquad (12)$$

where $\phi(\mathbf{r}) = \sum_k \psi_k(\mathbf{r}) c_k$, which yields

$$\rho(\mathbf{q}) = e^{-\frac{1}{4}\mathbf{q}^2 \ell_B^2} \int \frac{dk}{2\pi} \, e^{-i q_x k \ell_B^2} c^\dagger_{k-q_y/2} c_{k+q_y/2}. \qquad (13)$$

If the $y$-translational symmetry is unbroken, then $\langle c^\dagger_{k+q_y/2} c_{k-q_y/2} \rangle = n_k 2\pi \delta(q_y)$, where $n_k = \langle c^\dagger_k c_k \rangle$ is the momentum distribution. This leads, e.g., for a single mode along the $x$ axis $n_k = e^{iQk} n$ to

$$\langle \rho(\mathbf{q}) \rangle = 2\pi n e^{-\frac{1}{4} q_x^2 \ell_B^2} \delta(q_y) \delta\big(q_x \ell_B^2 - Q\big) \qquad (14)$$

which corresponds to a state which is uniform in the $y$-direction but has CDW order with wavevector $Q$ in the $x$-direction.

If the solution is translationally invariant, the resulting momentum independence of $G$ substantially simplifies Eqs. (9)–(11). Since in this case $W$ depends only on the difference between the leg momenta $k = k_1 - k_2$,

$$W_{kq}(iv) = \int dp \, e^{-ipk} \frac{U(p,q)}{1 - \Pi(iv)U(p,q)} \qquad (15)$$

with $U(p,q) = \frac{1}{\sqrt{p^2 + (q\ell_B^2)^2}} e^{-\frac{1}{2\ell_B^2}(p^2 + (q\ell_B^2)^2)}$, the polarization and self-energy become

$$\Pi(iv) = \frac{1}{\beta} \sum_{i\omega} G(i\omega + iv) G(i\omega) \qquad (16)$$

and

$$\Sigma(i\omega) = -\frac{1}{\beta} \sum_{iv} G(i\omega - iv) \mathcal{W}(iv), \qquad (17)$$

where

$$\mathcal{W}(iv) = \ell_B^2 \int_0^\infty d\rho \, \rho \frac{U(\rho)}{1 - \Pi(iv)U(\rho)} \qquad (18)$$

is a totally momentum independent effective interaction with $U(\rho) = e^{-\frac{1}{2}\rho^2 \ell_B^2}/\rho\ell_B^2$.

Let us first show that all solutions of Eqs. (7), (16), (17), and (18) are necessarily gapless in the $T = 0$ limit. Closely following the argument of Ref. [52] developed for the SYK model, let us assume that the Green's function has a gap $\Delta$, i.e., that the corresponding spectral function $\rho(\omega) = -\frac{1}{\pi} \mathrm{Im} \, G(\omega + i\eta)$ satisfies $\rho(\omega) = 0$ in some range of frequencies $|\omega| < \Delta/2$. By performing a spectral decomposition of Eqs. (16) and (17), it follows that $\mathcal{W}$ has a gap $2\Delta$ and that $\Sigma$ has a gap $3\Delta$, but then the Dyson equation (7) implies that the Green's function must have a gap $3\Delta$. Hence the only consistent value is $\Delta = 0$ and the solution is gapless.

Tunnelling experiments indicate that at low temperature, the electron spectral function exhibits a pseudogap (i.e., a strong suppression) at low frequencies [39–44]. This behavior has been found theoretically within the composite fermion picture, which yields an exponential suppression of the spectral function, $\rho(\omega) \propto e^{-\omega_0/|\omega|}$, with some energy scale $\omega_0 > 0$ [108,109]. Following a similar argument to that given above, it is possible to show that this spectral function is also inconsistent with the *GW* equations.

### A. Non-Fermi liquid solution

The set of equations (7), (16), (17), and (18) can be solved analytically for low frequencies and $T \to 0$, resulting in the nFL solution of the form (1). It corresponds to a broad singularity in the spectral function $\rho(\omega) = A|\omega|^{2\Delta-1}$ at low frequencies, which indicates an absence of well-defined electron-like quasiparticles, or, equivalently, an infinitesimally short quasiparticle lifetime. This self-energy, and thus the corresponding single-electron excitation spectrum, is the same as that of the nFL solution realized in the SYK model.

For $\omega \to 0$ the exponent $\Delta$ solves the equation (the calculation is outlined in Appendix C)

$$f(\Delta) + g(\Delta) \ln(\omega) = 1 \qquad (19)$$

with $f(\Delta)$ and $g(\Delta)$ being functions of $\Delta$ only, and

$$g(\Delta) = \frac{(4\Delta - 1)^2}{(2\Delta - 1)[\sec(2\pi\Delta) - 1]} \frac{\sin(\pi\Delta)^2}{\sin(\pi\Delta - \theta)\sin(\pi\Delta + \theta)}. \qquad (20)$$

Thus $g(\Delta) \to 0$ for $\omega \to 0$, which yields $\Delta = 1/4$ (and $f(\Delta) = 0$) for all $\theta$. The independence of $\Delta$ on the filling fraction is a nontrivial result, and in this case, is a consequence of the logarithmic corrections. To see this, note that the logarithm in the second term on the RHS of Eq. (19) implies that the solutions to Eq. (19) are given by the roots of the function $g(\Delta)$, which are robust with respect to variations of $\theta$. Without the logarithmic term in Eq. (19), the solution $\Delta$ is no longer a root of the function $g(\Delta)$, and therefore it acquires some weak dependence on $\theta$.

In practice, the asymptotic form Eq. (19) is applicable only for frequencies as small as $\omega \ll 10^{-6}$. In more practical frequency regimes we must solve the *GW* equations numerically. To this end, we examine the functions

$$\Delta_\Sigma(i\omega) = \frac{\partial \ln(|\Sigma(i\omega)|)}{\partial \ln(\omega)}, \quad \Delta_G(i\omega) = \frac{\partial \ln(|G(i\omega)|)}{\partial \ln(\omega)} \qquad (21)$$
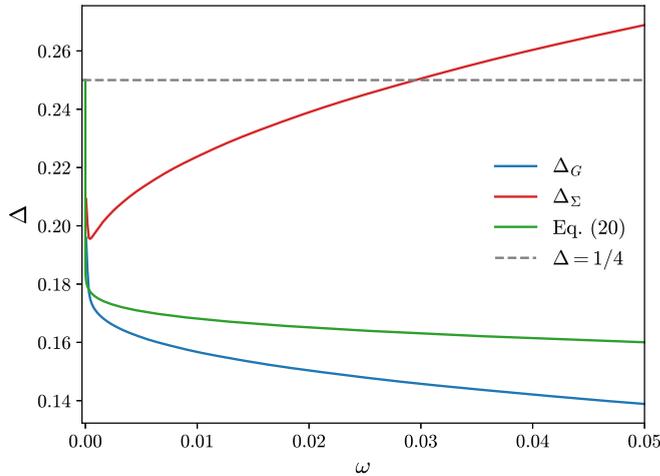
FIG. 2. The exponent $\Delta$ estimated from the functions $\Delta_G$ (blue curve) and $\Delta_\Sigma$ (red curve) defined in Eq. (21) at half-filling $\nu = 1/2$ ($\mu$, $\theta = 0$). This is shown for temperature $T = 2 \times 10^{-5}$. Finite temperature effects are seen at small frequencies $T \lesssim \omega \lesssim 10T$ as rapid up-turns. As $\omega \to 0$, the two curves approach asymptotically. Also shown (green curve) is the value of $\Delta$ that solves Eq. (19). At arbitrarily low-frequency, all three curves will coincide, and approach the value $\Delta = 1/4$ as $\omega \to 0$.

against frequency at the lowest accessible temperatures (in practice, $T = 2 \times 10^{-5}$) and at half-filling ($\mu = \theta = 0$). Since $G$ and $\Sigma$ are related by the Dyson equation (7), $\Delta_G$ and $\Delta_\Sigma$ will lead to the same estimate of $\Delta$ for sufficiently small $\omega$.

The result is shown in Fig. 2. It is clear that, for realistic frequencies, the deviation of the apparent $\Delta(\omega)$ from 1/4 due to the logarithmic in frequency corrections is substantial, meaning that the asymptotic value $\Delta = 1/4$ is not observable in practice. There are also notable differences between the estimates of $\Delta$ from the asymptotics of $G(i\omega)$ and $\Sigma(i\omega)$, stemming from $G_0$ in the Dyson equation. As the frequency is lowered, however, this difference is seen to eventually become less important compared to the remaining logarithmic corrections.

The nFL character [i.e., the anamolous scaling of $\Sigma(i\omega)$] of the solution will only be present at sufficiently low temperatures. At sufficiently high temperature, the system is in a free-fermion thermal state. To estimate the crossover temperature to the nFL regime, we consider the function $\delta\Sigma = \text{Im } \Sigma(i\omega_0) - \text{Im } \Sigma(i\omega_1)$, where $\omega_0 = \pi T$ and $\omega_1 = 3\pi T$ are the lowest and first Matsubara frequencies, respectively, and adopt the convention in which a metallic state corresponds to $\delta\Sigma < 0$, while the thermal state has $\delta\Sigma > 0$. In these terms, the crossover temperature $T_{\text{nFL}}$ is defined by the equation $\delta\Sigma = 0$, which yields $T_{\text{nFL}} \sim 0.1e^2/\ell_B$ roughly independent of the filling fraction, as indicated in Fig. 1.

The appearance of SYK physics in the microscopic description of the LLL could be seen as surprising. Qualitatively, a connection can be made in terms of the constraints placed on the Green's function by the requirement of a homogeneous charge-density—which imply that all single particle properties are momentum independent—and the flat band nature of the noninteracting physics. Mathematically, the form of the
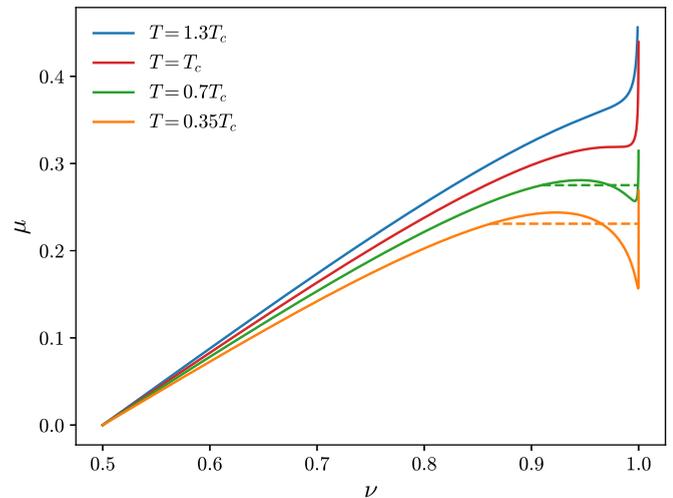


FIG. 3. Chemical potential $\mu$ against filling $\nu$ for various temperatures. The dashed lines, obtained using Maxwell's construction, show the value of $\mu$ at which the density jumps discontinuously as $\mu$ is varied in equilibrium.

SYK self-energy

$$\Sigma_{\text{SYK}}(i\omega) = -\frac{U^2}{\beta} \sum_\nu G(i\omega - i\nu)\Pi(i\nu), \qquad (22)$$

where $U$ is the SYK interaction strength and $\Pi$ is the polarization defined in Eq. (16), corresponds to that for the LLL, Eq. (17), with the single particle-hole bubble $\Pi$ in place of the full screened Coulomb interaction $W$. Therefore the SYK character of the $GW$ solution can be understood in terms of the dominance of the effect of the single-bubble contribution in $\mathcal{W}$, up to the logarithmic corrections due to the long-range nature of the bare Coulomb potential. Our preliminary calculations suggest that a similar nFL state is also present for the Trugman-Kivelson potential, for which the Laughlin wave function is the exact ground state [110]. A more focused study for this potential is left for future work.

While we have demonstrated that the single-particle excitation spectrum is (nearly) identical to that of the SYK model, it is possible that the multi-particle excitation spectrum, which is not investigated here, is distinct from that of the SYK model. For example the diagrammatic expansion for the density-density correlator—which determines the spectrum of two-particle excitations—that is thermodynamically consistent (in the Baym-Kadanoff sense [111]) with the $GW$ self-energy contains vertex corrections, while for the SYK model the vertex corrections vanish due to the large-$N$ limit [52,112]. Investigation of the two-particle spectrum for the current model is however beyond the scope of the present work.

### B. Phase diagram

Similarly to the SYK model [69,70], we find that a first-order transition to a band insulating phase, corresponding to a fully filled LLL, is triggered at some finite value $\mu_{\text{nFL-BI}}$. In Fig. 3, we show the chemical potential against density for different temperatures. The curves are obtained by fixing the
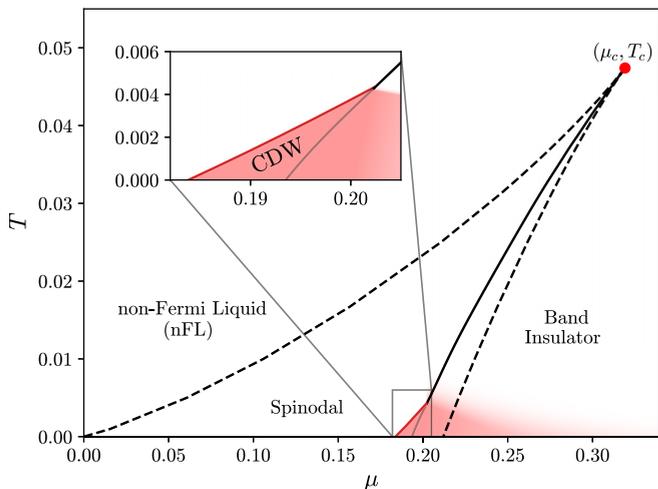
FIG. 4. Phase diagram in the $T$-$\mu$ plane. The solid black line marks the first order transition between the non-Fermi liquid and band-insulator phases at chemical potential $\mu_{\text{nFL-BI}}(T)$, which terminates at a critical end-point $(\mu_c, T_c)$ (red point). In the spinodal region, bounded by the dotted lines, both phases can be realized, however one is metastable. The second-order transition from the nFL to a charge-density wave is seen at low temperatures. On the band-insulator side, we expect the CDW to also be present, and for this to emerge from the band-insulator phase via a first-order phase transition. We have not determined the location of this transition, but indicate its presence by the blurred region.
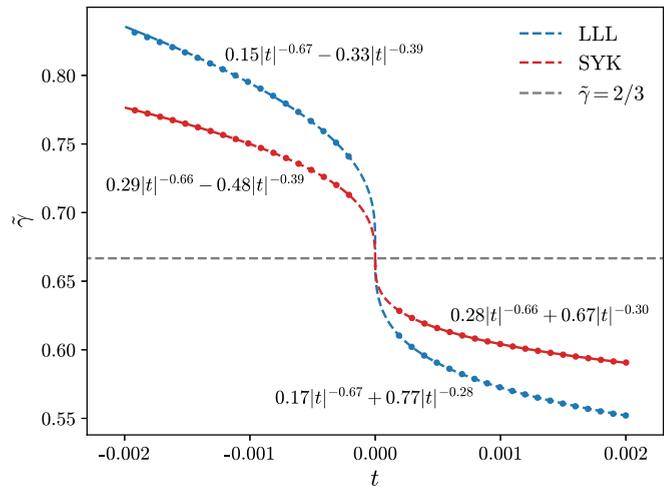


FIG. 5. Estimate of the susceptibility critical exponents $\tilde{\gamma}_\pm$. The function $\tilde{\gamma}(t)$, defined in Eq. (25), is plotted against the reduced temperature $t = (T - T_c)/T_c$ at the critical chemical potential $\mu_c$ for the lowest Landau level model (blue) and SYK model (red). The dashed lines are the fits by Eq. (26), revealing that the critical exponents for both LLL and SYK models and positive and negative $t$ are identical, and are in perfect agreement with the value $\tilde{\gamma} = 2/3$ obtained analytically for the $\text{SYK}_q$ model in the $q \to \infty$ limit in Ref. [71]. The fitting parameters for $f_{\text{fit}}(t)$, defined in Eq. (26), are shown next to their respective curves. The corrections to the critical scaling are asymmetric around $t = 0$, and $\tilde{\gamma}(t)$ approaches the limiting value $\tilde{\gamma}$ with infinite slope.

charge density $\nu$ and calculating the corresponding value of $\mu$. We observe the typical behavior of a first-order transition: below some critical temperature, we find a range of $\mu$ values for which three different solutions $\nu(\mu)$ exist. The solution with the intermediate charge density has a negative compressibility $K \propto \frac{d\nu}{d\mu} < 0$ and is therefore thermodynamically unstable. The chemical potential $\mu_{\text{nFL-BI}}$, at which $\nu$ jumps discontinuously, is found via Maxwell's construction (see Appendix D for details), depicted in Fig. 3 as the horizontal dashed line.

The phase diagram in the $T - \mu$ plane is shown in Fig. 4 (black solid and dotted curves). We focus solely on positive $\mu$, since the negative $\mu$ behavior can be inferred from the particle-hole symmetry. In the small-$\mu$ region, we find the nFL phase discussed in the previous section. In the large-$\mu$ region, the Green's function is exponential in imaginary time, $G(\tau > 0) \sim -e^{\mu\tau}$, for $\mu/T \gg 1$, which corresponds to a band-insulating phase with filling close to unity (at zero temperature the BI has strictly unit filling, while at finite temperature this phase exists for narrow range of fillings near unity due to thermal broadening effects). The two phases are separated by a first-order transition line, which ends at the second-order critical end point $(\mu_c, T_c)$. At all temperatures below $T_c$, there is some finite range of $\mu$, bounded by the dotted curves and labeled the spinodal region, in which both the nFL and BI solutions are found, but one is metastable. The critical parameters are $T_c = 0.04735(2)$, $\mu_c = 0.3190(1)$, which correspond to $\nu_c = 0.979(1)$.

The phase diagram in the $T$-$\nu$ plane is shown in Fig. 1. The solid black curve delimits the phase-separation region in which the nFL and band-insulating phases coexist. The critical point lies at the top of the phase-separation "dome."

## C. Critical point of the LLL and SYK models

We now focus on the critical point of the continuous transition, determine its universality class and compare the results to those for the SYK model. To this end, we calculate the critical exponents $\tilde{\gamma}_\pm$ of the compressibility $\chi(T, \mu) = \frac{\partial n}{\partial \mu}$ as a function of temperature, defined as

$$\chi(t, \mu_c) \sim |t|^{-\tilde{\gamma}_\pm} \text{ for } t \to 0^\pm \quad (23)$$

where $t = (T - T_c)/T_c$ is the reduced temperature, as well as the exponents $q_\pm$ for the density

$$|\nu(T, \mu_c) - \nu(T_c, \mu_c)| \sim |t|^{q_\pm} \text{ for } t \to 0^\pm. \quad (24)$$

The critical exponents can be evaluated by considering their temperature-dependent estimates

$$\tilde{\gamma}(t) = \frac{\partial \ln \chi(t, \mu_c)}{\partial \ln t}, \quad (25)$$

and similarly for $q(t)$. In previous studies of the critical point in the SYK model [69,70], the exponents $\tilde{\gamma}_\pm$, $q_\pm$ were obtained by a linear extrapolation of $\tilde{\gamma}(t)$, $q(t)$ to $t \to 0^\pm$. Since we have very small error bars on the critical values $\mu_c, T_c, \nu_c$, we are able to approach the critical point much more closely, observing that the limiting values of the critical exponents are actually approached with infinite slope (see Fig. 5). This results in significant error in the estimate if a linear extrapolation is performed, and indicates that leading-order corrections to the dominant power law are playing a significant role in the small-$t$ limit. We therefore use instead the fitting ansatz

$$f_{\text{fit}}(t) = a_\pm |t|^{\alpha_\pm} + b_\pm |t|^{\beta_\pm} \text{ for } t \to 0^\pm, \quad (26)$$

TABLE I. Critical parameters ($T_c$, $\mu_c$, $\nu_c$), critical exponents ($\tilde{\gamma}_+$, $\tilde{\gamma}_-$, $q_+$, $q_-$) and the corresponding sub-leading correction exponents ($\tilde{\gamma}_+^c$, $\tilde{\gamma}_-^c$, $q_+^c$, $q_-^c$) for both SYK$_4$ and LLL models. The subscript on the exponents specifies the direction in which the crtical point is approached.

| | $T_c$ | $\mu_c$ | $\nu_c$ | $\tilde{\gamma}_+$ | $\tilde{\gamma}_-$ | $q_+$ | $q_-$ | $\tilde{\gamma}_+^c$ | $\tilde{\gamma}_-^c$ | $q_+^c$ | $q_-^c$ |
|---|---|---|---|---|---|---|---|---|---|---|---|
| SYK$_4$ | 0.068372(2) | 0.344713(3) | 0.9498(2) | 0.66(1) | 0.66(1) | 0.33(1) | 0.33(1) | $-0.30(2)$ | $-0.35(4)$ | $-0.6(1)$ | $-0.65(5)$ |
| LLL | 0.04735(2) | 0.3190(1) | 0.3190(1) | 0.66(1) | 0.66(1) | 0.33(1) | 0.33(1) | $-0.29(2)$ | $-0.35(5)$ | $-0.65(5)$ | $-0.6(2)$ |

which is the simplest extension of a single power-law, and which includes the leading-order corrections to the critical behavior. To further reduce systematic errors from the use of a finite range of $t$ in the fit, we extract the fit parameters (including the value of $T_c$) for a set of different ranges of $t$ (with order of magnitude roughly $t \sim 10^{-4}$) and choices of $\mu_c$ within its error bar, and extrapolate the resulting values to the $t \to 0$ limit; the uncertainty of this extrapolation together with the spread of the data with $\mu_c$ is the source of the claimed error bars. An example of such a fit in the range $t \in [2 \times 10^{-4}, 2 \times 10^{-3}]$ is shown in Fig. 5. In this way, we obtain the critical exponents with high accuracy, as well as the exponents characterising the leading-order corrections. Since in Refs. [69,70] the exponents for the SYK model have been found to differ on the two sides of the transition, we calculate both independently.

The location of the critical point, as well as the critical exponents and subleading exponents for the LLL and SYK$_4$ models are summarized in Table I. For the LLL model we find the values $\tilde{\gamma}_+ = 0.66(1)$, $\tilde{\gamma}_- = 0.66(1)$ and $q_+ = 0.33(1)$, $q_- = 0.33(1)$. These exponents are different from those reported previously for the SYK$_4$ model. However, by evaluating the SYK$_4$ critical parameters with error bars at least two orders of magnitudes smaller than the previous estimates [$T_c^{\text{SYK}} = 0.068372(2)$, $\mu_c^{\text{SYK}} = 0.344713(3)$, and $\nu_c^{\text{SYK}} = 0.9498(2)$], and using the fit (26), we find the SYK$_4$ exponents $\tilde{\gamma}_+^{\text{SYK}} = 0.66(1)$, $\tilde{\gamma}_-^{\text{SYK}} = 0.66(1)$, and $q_+^{\text{SYK}} = 0.33(1)$, $q_-^{\text{SYK}} = 0.33(1)$, which are identical to our LLL exponents. Interestingly, while the exponents (both critical and correction) as well as the leading coefficients are symmetric around the critical point, we find that the coefficients of the sub-leading terms are asymmetric. This is likely the cause of the apparent asymmetry of the critical exponents obtained previously by linear fitting.

Very recently, an analytical study of the generalized SYK$_q$ model has been performed in the $q \to \infty$ limit [71]. The resulting exponents are identical to those obtained here for

the LLL and SYK (SYK$_4$ in these notations) models, and were found to belong to the Van der Waals/Ising mean-field universality class. It is emphasized by the authors of Ref. [71] that the critical exponents depend upon the direction in the $T$, $\mu$ plane along which the critical point is approached. This is the reason for the difference between the exponents given here and those usually quoted for this universality class (for more details on this topic, the reader is referred to Ref. [71]). Therefore we also conclude that both the LLL and the SYK$_4$ models belong to this universality class, and it is very likely that this is also true for all possible $q$ by continuity. A proper investigation of all SYK$_q$ critical points is beyond the present scope.

## V. *GW* CDW INSTABILITY

Having established the nature of the homogeneous phase, we now analyze the possibility of CDW instabilities within the *GW* approximation. We detect the occurrence of a continuous phase transition to a charge-ordered phase by the divergence of the charge susceptibility $\chi_P$ at the relevant wavevector $p$. We obtain $\chi_p$ via the Bethe-Salpeter equation, which is expressed in terms of the two-particle irreducible vertex $\Gamma$ (see Appendix A for the definition of the susceptibility). Since the *GW* approximation is $\Phi$-derivable, calculating $\Gamma$ via the functional derivative

$$\Gamma = \frac{1}{T} \frac{\delta \Sigma}{\delta G} \tag{27}$$

ensures thermodynamic consistency [111]. Determining the vertex in this way also allows a different interpretation of the divergence of the susceptibility: it signals the switchover from iterative stability to instability of a self-consistent solution of the Dyson equation. This is easily seen by linearising the Dyson equation around a solution. This viewpoint has also been adopted within dynamical mean field theory, wherein the variation with respect to the hybridization is considered [113,114]. Therefore our expression for the irreducible vertex within the *GW* approximation is represented diagrammatically as



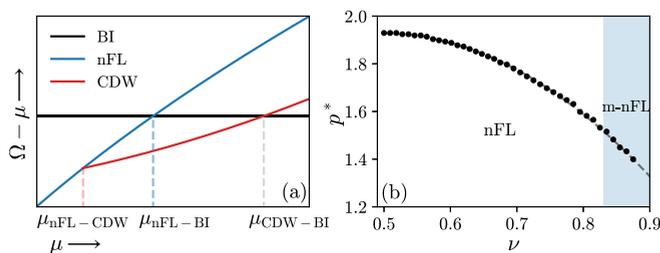$$\Gamma_{\omega\omega',kk'} = \tag{28}$$

FIG. 6. (a) Schematic illustration of the variation of the grand potential $\Omega$ with the chemical potential at constant (arbitrary) temperature $T$. The CDW curve must intersect the band-insulator (BI) curve at a chemical potential $\mu_{\text{CDW-BI}} \geqslant \mu_{\text{nFL-BI}}$, thus justifying the existence of the blurred region in Fig. 4 wherein the CDW exists. (b) The momentum $p^*$ at which the susceptibility is a maximum as a function of filling fraction $\nu$ at fixed temperature $T = 0.005$. In the shaded region, there are CDW transitions from the metastable nFL phase. In the pure nFL phase, there are no CDW transitions at this temperature. This shows no special features of the density fluctuations as the filling is varied.

where the dotted line represents $W$. In this expression, we set the transfer frequencies and momenta to zero since only these components are required to study the charge-density ordering instability. The index $k$ corresponds to position in the $x$ direction, and therefore we study the susceptibility as a function of the wave number $p$, which is the Fourier conjugate to $k$. Since we have a translation-invariant normal phase, implying dependence on only the difference $k - k'$, the Bethe-Salpeter equation for $\chi$ is diagonal in the wave-number basis.

The obtained critical temperature for the nFL-to-CDW transition as a function of the chemical potential is shown in Fig. 4 (red curve). We observe a small region at low temperature adjacent to the nFL-to-BI transition in which CDW order emerges. For $\mu \lesssim 0.18$ (corresponding to $0.5 \leqslant \nu \lesssim 0.8$), we find that the susceptibility roughly behaves as $\chi^{-1} \sim aT + C$, where $a, C$ are positive constants (with $C \to 0$ as $\mu \to 0.18$ or $\nu \to 0.8$), at the momentum at which $\chi^{-1}$ is the smallest. This suggests that no CDW transition takes place down to zero temperature below $\mu \approx 0.18$ ($\nu \approx 0.8$). Within the BI phase at $\mu \gtrsim 0.2$ ($\nu \approx 1$, almost independently of $\mu$) and at low temperatures, charge fluctuations are strongly suppressed, which eliminates the possibility of a continuous transition to a CDW in this region of the phase diagram. However, generically, the CDW should be present here too, separated from the BI phase by a first-order transition. This can be seen by considering the grand potentials of all three phases [nFL, CDW and BI, see an illustration in Fig. 6(a)]. At the nFL-to-CDW transition [red dashed line in Fig. 6(a) and red line in Fig. 4], the grand potential $\Omega_{\text{CDW}}$ of the CDW phase emerges below that of the nFL phase $\Omega_{\text{nFL}}$. This means $\Omega_{\text{CDW}}$ must be smaller than the BI grand potential, $\Omega_{\text{BI}}$, at the location of the first-order nFL-BI transition, where $\Omega_{\text{nFL}} = \Omega_{\text{BI}}$ [blue dashed line in Fig. 6(a) and black line in the inset of Fig. 4]. This implies that in general the CDW will persist into the BI region, undergoing a first-order transition to the BI phase at some chemical potential $\mu_{\text{CDW-BI}}$ [gray dashed line in Fig. 6(a)]. Detecting first-order transitions is beyond the present study, and thus we indicate the corresponding boundary of the CDW region only roughly by blurring in Figs. 1 and 4.

The CDW transition line is also shown in the temperature-density plane in Fig. 1. Between roughly $\nu = 0.8$ and $0.82$, the CDW emerges from the pure nFL phase via a second order phase transition. In the phase separation region $\nu \approx 0.82$ to $\nu \approx 1$, our calculated Green's functions, which correspond to a pure phase, do not capture the equilibrium properties of the system. Within the metastable nFL phase, the transition to the CDW is shown in Fig. 1 by the dashed red line. Generically, from the analysis of the grand potentials of the corresponding phases [Fig. 6(a)], we expect that the ground state in the phase-separation region is a CDW, with a (first-order) transition temperature that depends on the filling fraction.

We have investigated the wave-number dependence of $\chi$ at fixed temperature, by plotting the wave number $p_*$ at which $\chi$ is maximum as a function of $\nu$, as shown in Fig. 6(b) at temperature $T = 0.005$. Note that at this temperature, there are no CDW transitions from the pure nFL phase. However, transitions do occur from the metastable nFL phase at certain filling fractions, as marked in Fig. 6. This shows no special features as $\nu$ is varied, but we note that in contrast to Hartree-Fock, $p_*$ depends on $\nu$ and that where the CDW phase exists, the dependence of the ordering wave vector is very weak.

The phase diagram obtained in the Hartree-Fock approximation [33] is drastically different from our self-consistent $GW$ theory: the Hartree-Fock ground state is a CDW at all filling fractions, with a typical transition temperature an order of magnitude higher than that of the CDW state in $GW$. Because of its dynamically fluctuating nature, the nFL state, which dominates the phase diagram and suppresses the possibility of ordering, is entirely missed by the Hartree-Fock theory.

We also compare our results to the experimental critical temperatures [68]. We find that the values of filling and temperature for the onset of the CDW phase are in qualitative agreement with experiment. Therefore, while the $GW$ approximation does not capture the low-temperature FQH states at odd-denominator fillings in the range $0.2 \lesssim \nu \lesssim 0.8$, qualitative agreement with experiment is achieved outside this range of $\nu$. An explanation for this agreement could lie in the fact that $GW$, being controlled in the large-$\mu$ limit, is intrinsically more accurate at larger filling fractions.

## VI. DISCUSSION

We have analysed the microscopic model of electrons in the lowest Landau level interacting via the Coulomb potential by the self-consistent (skeleton) diagrammatic theory truncated at the level of the $GW$ approximation. Our central observation is a peculiar finite-temperature nFL state, realized in a wide range of LLL filling fractions, $0.2 \lesssim \nu \lesssim 0.8$. The state is qualitatively similar to that found in the paradigmatic SYK model and features a power-law—rather than linear as in a Fermi liquid—frequency dependence of the self-energy at low frequencies. We demonstrate that the anomalous dimension, which characterizes this power-law, deviates from that in the SYK model by sizable logarithmic corrections due to the Coulomb interaction. The SYK-like nFL state exhibits transitions to different insulating states at low temperatures. At large (or small, by particle-hole symmetry) fillings, we observe a first-order transition from the nFL state to a band insulator phase corresponding to a full (or empty) LLL, with

a critical end point. The critical point is found to belong to the same universality class as its counterpart in the $\text{SYK}_q$ models for all $q$, which itself is determined to be in the Van der Waals universality class. Near the nFL-BI transition, the nFL state also exhibits a second-order instability towards CDW order in a narrow range of filling fractions $0.8 \lesssim \nu \lesssim 0.82$ and at low temperatures, which are qualitatively consistent with those observed for CDW ordering experimentally.

Notably, in the wide range $0.2 \lesssim \nu \lesssim 0.8$, the nFL phase remains stable down to the ground state and the fractional quantum Hall (FQH) states at odd denominator fillings are not observed within the *GW* theory. In fact, we demonstrate that the fully self-consistent *GW* approximation necessarily gives a gapless phase if the solution is assumed translation-symmetric, as is the case for a FQH state. One implication of this fact is that the Tao-Thouless states [36,37], found earlier by a *GW* theory similar to the quasiparticle self-consistent *GW* approximation [105–107], are in fact not valid in the fully consistent case.

At even-denominator filling fractions, experiments indicate a metallic state at low temperatures, which at first glance seems consistent with our observations at these fillings. However, the nFL state we observe is of a fundamentally different character to the experimentally observed Fermi liquid states of composite fermions. This is clear from the studies of tunneling between two parallel electron planes in the high magnetic field limit [39–44], which directly probe the spectral function $\rho(\omega)$ of the electrons in the partially filled LLL. It was found that, for the even-denominator compressible states, $\rho(\omega)$ exhibits an 'orthogonality catastrophe' at low temperature, i.e., a strong (exponential) suppression of $\rho(\omega)$ at $\omega \to 0$. Similar features are obtained theoretically using the composite fermion approach [108,109], by a classical treatment of the electron liquid [115] and by approximating the system as a Wigner crystal (which is thought to accurately capture the short-range correlations) [116], as well as numerically for small numbers of electrons [117]. Despite the suppression of $\rho(0)$, the system exhibits metallic transport properties because the conducting quasiparticles are not the microscopic electrons but rather the composite fermions, which have little overlap with the electrons [118]. From these considerations, it is evident that extending the microscopic theory beyond the *GW* approximation is necessary to capture the experimentally observed behavior of the partially filled LLL at very low temperatures.

Calculations that would systematically include diagrams beyond *GW*, e.g., by means of diagrammatic Monte Carlo techniques [47–51], are also needed to evaluate the systematic errors of our results. Nonetheless, since the *GW* approximation is controlled in the limit of high temperatures and correctly captures the thin-torus limit at all temperatures, we expect that the nFL phase found here at intermediate temperatures should be observable in the LLL system. It would exist within an intermediate range of temperatures below the free-fermion thermal state to non-Fermi liquid crossover temperature $T_{\text{nFL}} \sim 0.1 e^2/\ell_B \sim 20$ K, but above the temperature at which the correlations present in the FQH state begin to develop, which roughly could be taken as at most the gap scale $T_{\text{gap}} \sim 0.05 e^2/\ell_B \sim 10$ K [119], where the temperatures in kelvin are shown for the typical magnetic field strength

$B = 13$ T. If this is the case, then the FQH states, and indeed the metallic states at even denominators, could emerge from this state of incoherent electrons as the temperature is lowered. While direct calculation of the resistivity for the LLL model is left for future studies, we conjecture that, experimentally, a signature of this nFL phase could be an anomalous scaling of the resistivity with temperature of the form $\rho_{\text{dc}}(T) \sim T^{2-4\Delta}$ with $\Delta$ the anomalous dimension defined in Eq. (1), as is found for models of itinerant electrons exhibiting an SYK-like phase [112]. In the LLL model, the value $\Delta = 1/4$ is only valid in the strict $\omega \to 0$ limit, meaning that at finite temperatures the substantial logarithmic corrections to $\Delta$ would likely lead to observable deviations from the linear-in-$T$ behavior expected for $\Delta = 1/4$. While experimental results exist for the variation of the resistivity with the temperature [45,120], the temperatures ranges are low and the system is in the FQH regime. As far as we are aware, experimental data at higher temperatures does not yet exist in the literature. Our results suggest that the physics at these intermediate temperatures is potentially very rich and its further investigation can shed new light on the nature of the FQH states.

## APPENDIX A: HARTREE-FOCK CDW INSTABILITY

### 1. Detecting CDW instability

The susceptibility of the system can be defined by considering the following extra term in the Hamiltonian:

$$H'(\tau) = -\sum_k \zeta_k(\tau) c_k^\dagger(\tau) c_k(\tau), \tag{A1}$$

where $\zeta_k(\tau)$ is an momentum dependent external field. Since this is an imaginary-time dependent perturbation, its action is to bring the system out of equilibrium. However, we are only interested in the limit $\zeta \to 0$, which restores thermodynamic equilibrium. The relevant susceptibility is the density-density correlator

$$\chi_{k-k'}(\tau - \tau') = \frac{1}{\beta} \left. \frac{\delta\langle n_k(\tau)\rangle}{\delta\zeta_{k'}(\tau')} \right|_{\zeta_{k'} \to 0}$$
$$= \langle n_k(\tau) n_{k'}(\tau')\rangle - \langle n_k\rangle\langle n_{k'}\rangle \tag{A2}$$

[the numerator $\langle n_k(\tau)\rangle$ is time-dependent because we have not yet taken the limit $\zeta \to 0$]. The static part of the Fourier transform (with respect to $k - k'$) $\chi_p(i\nu = 0)$ with wave number $p$ diverges at the (second-order) phase transition between the homogeneous and CDW phases.

We calculate the static response $\chi_{k-k'}(i\nu = 0)$ by considering the generalized susceptibility, which in particle-hole notation for the frequency dependence can be expressed in terms of the (particle-hole) irreducible vertex $\Gamma_{ph}$ via the following Bethe-Salpeter equation

$$\chi^{\omega\omega'\nu} = \chi_0^{\omega\omega'\nu} - \frac{1}{\beta^2} \sum_{\omega_1\omega_2} \chi_0^{\omega\omega_1\nu} \Gamma_{ph}^{\omega_1\omega_2\nu} \chi^{\omega_2\omega'\nu}, \tag{A3}$$

where $\chi_0^{\omega\omega'\nu} = -\beta G(i\omega)G(i\omega' + i\nu)\delta_{\omega\omega'}$ is the bare susceptibility and we have suppressed momentum indices for now (we use similar notations and definitions to those found in Ref. [121]). Since the CDW response function is static we will only consider the $\nu = 0$ components of $\chi$. As a matrix equation, Eq. (A3) becomes

$$\chi = \frac{\chi_0}{1 + T^2 \chi_0 \Gamma}. \tag{A4}$$

The vertex $\Gamma_{kk'}$ can be written in terms of $G$ and $\Sigma$ as (considering only the $\nu = 0$, $q = 0$ components)

$$\Gamma_{\omega\omega',kk'} = \frac{1}{T}\frac{\delta\Sigma_{k,\omega}}{\delta G_{k',\omega'}}. \tag{A5}$$

Since the normal phase is translation invariant and in the LLL model the momentum $k$ corresponds to position (in the $x$ direction), we have $\Gamma_{kk'} = \Gamma_{k-k'}$, which can be seen by explicit calculation. Therefore the inverse susceptibility can be written in terms of the wave number $p$ as

$$(\chi^{-1})_{\omega\omega',p} = -T\frac{1}{G(i\omega)^2}[\delta_{\omega,\omega'} - TG(i\omega)^2\Gamma_{\omega\omega',p}]. \tag{A6}$$

If $(\chi^{-1})_{\omega\omega',p}$ has a zero eigenvalue, then this implies that the response function

$$\chi_p = \frac{1}{\beta^2}\sum_{\omega,\omega'}\chi_{\omega\omega',p} \tag{A7}$$

is divergent. We can therefore calculate the eigenvalues of $(\chi^{-1})_{\omega\omega',p}$ and determine the critical point as the point at which an eigenvalue vanishes.

### 2. CDW in the Hartree-Fock approximation

At the level of the Hartree-Fock (mean-field) approximation, it is possible to find the critical point analytically without considering the eigenvalues. Since the self-energy is frequency-independent, the self-energy (8) only depends on momentum:

$$\xi_k = \int \frac{dq}{2\pi}(V_{k-q,0} - V_{0,k-q})n_F(\xi_q - \mu) \tag{A8}$$

where $n_F(x) = (e^{\beta x} + 1)^{-1}$ is the Fermi function. Introducing a wave-number label $p$ and Fourier transforming this equation gives

$$\xi_p = U_p n_p, \tag{A9}$$

where

$$n_p = \int \frac{dq}{2\pi}e^{ipq}n_F(\xi_q - \mu) \tag{A10}$$

and the effective potential is

$$U_p = \frac{1}{|p|}e^{-\frac{p^2}{2\ell_B^2}} - \sqrt{\frac{\pi}{2\ell_B^2}}e^{-\frac{p^2}{4\ell_B^2}}I_0\left(\frac{p^2}{4\ell_B^2}\right), \tag{A11}$$

where $I_0$ is the modified Bessel function of the first kind. We therefore have a set of decoupled modes, which correspond to different wavelength charge density waves, as discussed in Section II. Specifically, $\Gamma_{\omega\omega',p} = U_p$ in the Hartree-Fock approximation, and we can write the Bethe-Salpeter equation for

$\chi$ in terms of the wave number $p$ as

$$\chi_{\omega\omega',p} = -\beta G^2(i\omega)\delta_{\omega\omega'} + \frac{1}{\beta}\sum_{\omega_1}G(i\omega)^2 U_p \chi_{\omega_1\omega',p} \tag{A12}$$

from which it follows that the physical response $\chi_p = \frac{1}{\beta^2}\sum_{\omega\omega'}\chi_{\omega\omega',p}$ is

$$\chi_p = \frac{\beta\nu(1-\nu)}{1 + \beta U_p \nu(1-\nu)}, \tag{A13}$$

which is the usual expression for the RPA density-density response. Since $U_p$ has a negative minimum at $p* = 1.568$ with value $U_{p*} = -0.557$, we have a critical temperature

$$T_c = 0.557\nu(1-\nu) \tag{A14}$$

below which the system is unstable to the formation of a CDW with wave vector $p*$.

Using the fact that the critical temperature is $T_c = -U_p\nu(1-\nu)$, we can rewrite Eq. (A13) as

$$\chi_p = \frac{\nu(1-\nu)}{T - T_c}, \tag{A15}$$

which gives the critical exponent $\gamma_+ = 1$ where $\chi_p \sim |T - T_c|^{-\gamma_+}$ for $T \to T_c^+$.

In addition to this second order phase transition, it is known that Hartree-Fock also gives first order transitions with a slightly higher transition temperature away from half-filling [33]. In addition, the ordering momentum is lowered as one moves away from half-filling.

### APPENDIX B: TAO-THOULESS THEORY AND TT LIMIT

Equations (7), (9) (10), and (11) were solved approximately by Tao and Thouless [36,37]. For filling fraction $\nu = \frac{1}{q}$, they approximate the self-energy to be frequency independent and periodic in momentum with period $q$ in units of the momentum spacing (it is not clear how to interpret this in the thermodynamic limit, since then the spacing vanishes). Under these assumptions, it is shown that the system is gapped for all $q$, including for $q$ even. This shortcoming of the theory as well as some others [122,123] meant that this picture was quickly abandoned as a correct description. In addition, their solution is not fully self-consistent, but instead relies on a quasiparticle type self-consistency, which approximates the full self-energy by its lowest-frequency value. By extending their calculation to include full self-consistency, we have found that the frequency dependence of $\Sigma$ destroys the gap and leads to solutions that are momentum independent. Therefore we conclude that the TT-type ansatz is not a valid solution at the level of fully self-consistent $GW$.

The Tao-Thouless theory is now known to be relevant for the quantum Hall system in the so-called thin torus (TT) limit [79–82]. On a torus with small circumference $L_y \to 0$, the Hamiltonian can be solved exactly and one obtains gapped CDW states for the odd-denominator filling $\nu = 1/q$. These states have the same qualitative properties as the Laughlin states, such as fractionally charged excitations and ground state degeneracy $q$ on the torus. These CDW states are also observed for even denominators in the strict $L_y \to 0$, but as $L_y$ is

increased (to roughly $L_y = 5$) they are seen to undergo a quantum phase transition to a metallic state of neutral fermions that suggests a one-dimensional luttinger liquid description [79]. The CDW states for odd $q$ and the Luttinger liquid states for even $q$ are then conjectured to be adiabatically connected to the states in the experimentally relevant limit $L_y \to \infty$, which is also supported numerically [90].

## APPENDIX C: NON-FERMI LIQUID SOLUTION

To solve Eqs. (7), (16), (17), and (18) we assume a power-law form of the self-energy

$$\Sigma(i\omega) = \lambda e^{-i\text{sign}(\omega)(\pi/2+\theta)}|\omega|^{1-2\Delta}, \quad \omega \to 0 \quad \text{(C1)}$$

with $0 < \Delta < 1/2$, $\lambda > 0$ and particle-hole asymmetry parameter $-\pi\Delta < \theta < \pi\Delta$. For this range of $\Delta$, $\Sigma$ dominates the bare Green's function in the Dyson equaton, and hence the corresponding Green's function is

$$G(i\omega) = -\frac{1}{\lambda} e^{i\text{sign}(\omega)(\pi/2+\theta)}|\omega|^{-(1-2\Delta)}, \quad \omega \to 0. \quad \text{(C2)}$$

In the time-domain, this corresponds to

$$G(\tau) = -\frac{\Gamma(2\Delta)\sin(\pi\Delta - \text{sign}(\tau)\theta)\,\text{sign}(\tau)}{\pi\lambda|\tau|^{2\Delta}} \quad \text{(C3)}$$

and hence

$$\Pi(\tau) = -\frac{\Gamma(2\Delta)^2 \sin(\pi\Delta - \theta)\sin(\pi\Delta + \theta)}{\pi^2\lambda^2}\frac{1}{|\tau|^{4\Delta}}. \quad \text{(C4)}$$

Noting the identity

$$\int_{-\infty}^{\infty} \frac{1}{|x|^\alpha} e^{i\omega x} dx = \frac{2\sin\left(\frac{\pi\alpha}{2}\right)\Gamma(1-\alpha)}{|\omega|^{1-\alpha}} \quad \text{for } 0 < \alpha < 1, \quad \text{(C5)}$$

we see that if $0 < \Delta < \frac{1}{4}$, then

$$\Pi(i\nu) = \int_{-\infty}^{\infty} d\tau \, e^{i\nu\tau} \Pi(\tau) = -\frac{1}{\lambda^2}C_\Delta|\nu|^{4\Delta-1}, \quad \nu \to 0 \quad \text{(C6)}$$

with the constant

$$C_\Delta = \frac{4}{\pi^2}\sin(\pi\Delta)\sin(\pi\Delta - \theta)\sin(\pi\Delta + \theta)\cos(\pi\Delta)$$
$$\times \Gamma(1-4\Delta)\Gamma(2\Delta)^2. \quad \text{(C7)}$$

Note that in order for $\text{Re}\,\Pi(i\nu)$ to be strictly negative (as required by the spectral representation), $C_\Delta$ must be positive

which is consistent with the restriction $0 < \Delta < 1/4$. Note that this also implies $\Pi(i\nu \to 0) \to -\infty$.

Equation (9) can be rewritten as

$$\mathcal{W}(i\nu) = \frac{\lambda^2}{C_\Delta|\nu|^{4\Delta-1}}\int_0^\infty d\rho\,\rho\frac{\lambda^{-2}C_\Delta|\nu|^{4\Delta-1}}{e^{\frac{1}{2}\rho^2}\rho + \lambda^{-2}C_\Delta|\nu|^{4\Delta-1}}. \quad \text{(C8)}$$

At small $\nu$, the term $\lambda^{-2}C_\Delta|\nu|^{4\Delta-1}$ in the denominator dominates the other term for values of $\rho \ll \Lambda$ where $\Lambda e^{\frac{1}{2}\Lambda^2} = \lambda^{-2}C_\Delta|\nu|^{4\Delta-1}$. The integrand for $\rho \gg \Lambda$ is vanishingly small. Therefore, we utilize $\Lambda$ as a hard UV cutoff as follows:

$$\mathcal{W}(i\nu) = \frac{\lambda^2}{C_\Delta|\nu|^{4\Delta-1}}\int_0^\Lambda d\rho\,\rho = \frac{\lambda^2}{C_\Delta|\nu|^{4\Delta-1}}\frac{\Lambda^2}{2}. \quad \text{(C9)}$$

In the limit $\nu \to 0$, the equation $\Lambda e^{\frac{1}{2}\Lambda^2} = \lambda^{-2}C_\Delta|\nu|^{4\Delta-1}$ has the asymptotic solution

$$\Lambda^2 = \ln\left(\frac{(C_\Delta|\nu|^{4\Delta-1})^2}{2\lambda^4\ln\left(\frac{C_\Delta|\nu|^{4\Delta-1}}{\lambda^2}\right)}\right). \quad \text{(C10)}$$

Ignoring the double-log term, which is sub-leading as $\nu \to 0$, this yields

$$\mathcal{W}(i\nu) = \frac{\lambda^2}{C_\Delta|\nu|^{4\Delta-1}}\ln\left(\frac{C_\Delta|\nu|^{4\Delta-1}}{\lambda^2}\right), \quad \nu \to 0. \quad \text{(C11)}$$

Moving to the real-frequency axis, we find

$$\text{Im}\,\mathcal{W}(\nu + i\eta) = -\lambda^2 B_\Delta \nu^{1-4\Delta} - \lambda^2 D_\Delta(4\Delta - 1)\nu^{1-4\Delta}\ln(\nu), \quad \text{(C12)}$$

where

$$B_\Delta = \frac{\sin\left(\frac{\pi}{2}(1-4\Delta)\right)\ln\left(\frac{C_\Delta}{\lambda^2}\right)}{C_\Delta} + \frac{\pi}{2C_\Delta}(1-4\Delta)\cos\left(\frac{\pi}{2}(1-4\Delta)\right), \quad \text{(C13)}$$

$$D_\Delta = \frac{\sin\left(\frac{\pi}{2}(1-4\Delta)\right)}{C_\Delta}. \quad \text{(C14)}$$

On the real-frequency axis, the imaginary-part of the self-energy is given by

$$\text{Im}\,\Sigma(\omega) = \int_0^\omega d\Omega\,\text{Im}\,\mathcal{W}(\omega - \Omega)\rho(\Omega) \quad \text{(C15)}$$

where $\omega > 0$. Performing the integration yields

$$\text{Im}\,\Sigma(\omega) = -\lambda\sin(\pi\Delta - \theta)\omega^{1-2\Delta}\frac{\Gamma(2-4\Delta)\Gamma(2\Delta)}{\pi\Gamma(2-2\Delta)}\left[B_\Delta + D_\Delta(4\Delta - 1)\left(\frac{\Gamma'(2-4\Delta)}{\Gamma(2-4\Delta)} - \frac{\Gamma'(2-2\Delta)}{\Gamma(2-2\Delta)} + \ln(\omega)\right)\right] \quad \text{(C16)}$$

for $\omega > 0$. Comparing this to Eq. (C1) on the real frequency axis then gives the equation

$$f(\Delta) + g(\Delta)\ln(\omega) = 1 \quad \text{(C17)}$$

with $g(\Delta)$ defined in Eq. (20) and

$$f(\Delta) = \frac{\Gamma(2-4\Delta)\Gamma(2\Delta)}{\pi\Gamma(2-2\Delta)}\left[B_\Delta + D_\Delta(4\Delta - 1)\left(\frac{\Gamma'(2-4\Delta)}{\Gamma(2-4\Delta)} - \frac{\Gamma'(2-2\Delta)}{\Gamma(2-2\Delta)}\right)\right]. \quad \text{(C18)}$$

In the limit $\omega \to 0$, Eq. (C17) is solved by $g(\Delta) = 0$, yielding $\Delta = \frac{1}{4}$. Note, for this to be a good approximation, the cutoff needs to satisfy $\Lambda \gg 2$. This corresponds to a frequency of around $\nu \ll 10^{-6}$ for the expected values of $\Delta$.

## APPENDIX D: MAXWELL CONSTRUCTION

We find the chemical potential $\mu_{\text{nFL-BI}}$ of the coexistence of the nFL and BI phases across the first-order transition as follows. Equilibrium between point $A$ in one phase and point $B$ in the other phase occurs when the grand potentials of the two phases are equal: $\Omega_A = \Omega_B$. Considering the points $A$ and $B$ to be at the same temperature $T$ and volume $V$, the equilibrium condition can be expressed via an integral of $(d\Omega)_{T,V} = -N d\mu$ from $A$ to $B$. However, since the function $N(\mu)$ is multivalued, we first Legendre transform $\Omega$ to the free energy $F = \Omega + \mu N$, and compute its (isothermal and isochoric) change as

$$F_B - F_A = \int_{N_A}^{N_B} \mu(N) dN, \tag{D1}$$

where the equilibrium between the two phase requires $\mu(N_A) = \mu(N_B) \equiv \mu_{\text{nFL-BI}}$. Thus, going back to the grand potential, we obtain

$$\Omega_B - \Omega_A = F_B - F_A - \mu(N_B)N_B + \mu(N_A)N_A$$
$$= \int_{N_A}^{N_B} (\mu(N) - \mu_{\text{nFL-BI}}) dN = 0, \tag{D2}$$

the solution to which determines $\mu_{\text{nFL-BI}}$.

[1] D. C. Tsui, H. L. Stormer, and A. C. Gossard, Two-dimensional magnetotransport in the extreme quantum limit, Phys. Rev. Lett. **48**, 1559 (1982).

[2] H. L. Stormer, A. Chang, D. C. Tsui, J. C. M. Hwang, A. C. Gossard, and W. Wiegmann, Fractional quantization of the Hall effect, Phys. Rev. Lett. **50**, 1953 (1983).

[3] D. Arovas, J. R. Schrieffer, and F. Wilczek, Fractional statistics and the quantum Hall effect, Phys. Rev. Lett. **53**, 722 (1984).

[4] B. I. Halperin, Statistics of quasiparticles and the hierarchy of fractional quantized Hall states, Phys. Rev. Lett. **52**, 1583 (1984).

[5] R. B. Laughlin, Anomalous quantum Hall effect: An incompressible quantum fluid with fractionally charged excitations, Phys. Rev. Lett. **50**, 1395 (1983).

[6] J. K. Jain, Composite-fermion approach for the fractional quantum Hall effect, Phys. Rev. Lett. **63**, 199 (1989).

[7] J. K. Jain, Theory of the fractional quantum Hall effect, Phys. Rev. B **41**, 7653 (1990).

[8] A. Lopez and E. Fradkin, Fractional quantum Hall effect and Chern-Simons gauge theories, Phys. Rev. B **44**, 5246 (1991).

[9] S. C. Zhang, T. H. Hansson, and S. Kivelson, Effective-field-theory model for the fractional quantum Hall effect, Phys. Rev. Lett. **62**, 82 (1989).

[10] B. I. Halperin, P. A. Lee, and N. Read, Theory of the half-filled Landau level, Phys. Rev. B **47**, 7312 (1993).

[11] R. Shankar and G. Murthy, Towards a field theory of fractional quantum Hall states, Phys. Rev. Lett. **79**, 4437 (1997).

[12] H. W. Jiang, H. L. Stormer, D. C. Tsui, L. N. Pfeiffer, and K. W. West, Transport anomalies in the lowest Landau level of two-dimensional electrons at half-filling, Phys. Rev. B **40**, 12013 (1989).

[13] R. L. Willett, M. A. Paalanen, R. R. Ruel, K. W. West, L. N. Pfeiffer, and D. J. Bishop, Anomalous sound propagation at $\nu=1/2$ in a 2D electron gas: Observation of a spontaneously broken translational symmetry? Phys. Rev. Lett. **65**, 112 (1990).

[14] R. L. Willett, R. R. Ruel, M. A. Paalanen, K. W. West, and L. N. Pfeiffer, Enhanced finite-wave-vector conductivity at multiple even-denominator filling factors in two-dimensional electron systems, Phys. Rev. B **47**, 7344 (1993).

[15] W. Kang, H. L. Stormer, L. N. Pfeiffer, K. W. Baldwin, and K. W. West, How real are composite fermions? Phys. Rev. Lett. **71**, 3850 (1993).

[16] R. L. Willett, R. R. Ruel, K. W. West, and L. N. Pfeiffer, Experimental demonstration of a Fermi surface at one-half filling of the lowest Landau level, Phys. Rev. Lett. **71**, 3846 (1993).

[17] R. R. Du, H. L. Stormer, D. C. Tsui, L. N. Pfeiffer, and K. W. West, Experimental evidence for new particles in the fractional quantum Hall effect, Phys. Rev. Lett. **70**, 2944 (1993).

[18] R. L. Willett, Experimental evidence for composite fermions, Adv. Phys. **46**, 447 (1997).

[19] D. Yoshioka, B. I. Halperin, and P. A. Lee, Ground state of two-dimensional electrons in strong magnetic fields and $\frac{1}{3}$ quantized Hall effect, Phys. Rev. Lett. **50**, 1219 (1983).

[20] R. B. Laughlin, Quantized motion of three two-dimensional electrons in a strong magnetic field, Phys. Rev. B **27**, 3383 (1983).

[21] F. D. M. Haldane, Fractional quantization of the Hall effect: A hierarchy of incompressible quantum fluid states, Phys. Rev. Lett. **51**, 605 (1983).

[22] F. D. M. Haldane and E. H. Rezayi, Finite-size studies of the incompressible state of the fractionally quantized Hall effect and its excitations, Phys. Rev. Lett. **54**, 237 (1985).

[23] G. Fano, F. Ortolani, and E. Colombo, Configuration-interaction calculations on the fractional quantum Hall effect, Phys. Rev. B **34**, 2670 (1986).

[24] N. d'Ambrumenil and R. Morf, Hierarchical classification of fractional quantum Hall states, Phys. Rev. B **40**, 6108 (1989).

[25] R. H. Morf, N. d'Ambrumenil, and S. Das Sarma, Excitation gaps in fractional quantum Hall states: An exact diagonalization study, Phys. Rev. B **66**, 075408 (2002).

[26] N. Shibata and D. Yoshioka, Ground-state phase diagram of 2D electrons in a high Landau level: A density-matrix renormalization group study, Phys. Rev. Lett. **86**, 5755 (2001).

[27] A. E. Feiguin, E. Rezayi, C. Nayak, and S. Das Sarma, Density matrix renormalization group study of incompressible fractional quantum Hall states, Phys. Rev. Lett. **100**, 166803 (2008).

[28] D. L. Kovrizhin, Density matrix renormalization group for bosonic quantum Hall effect, Phys. Rev. B **81**, 125130 (2010).

[29] M. P. Zaletel and R. S. K. Mong, Exact matrix product states for quantum Hall wave functions, Phys. Rev. B **86**, 245305 (2012).

[30] Z.-X. Hu, Z. Papić, S. Johri, R. Bhatt, and P. Schmitteckert, Comparison of the density-matrix renormalization group method applied to fractional quantum Hall systems in different geometries, Phys. Lett. A **376**, 2157 (2012).

[31] B. Estienne, Z. Papić, N. Regnault, and B. A. Bernevig, Matrix product states for trial quantum Hall states, Phys. Rev. B **87**, 161112(R) (2013).

[32] M. P. Zaletel, R. S. K. Mong, and F. Pollmann, Topological characterization of fractional quantum Hall ground states from microscopic hamiltonians, Phys. Rev. Lett. **110**, 236801 (2013).

[33] H. Fukuyama, P. M. Platzman, and P. W. Anderson, Two-dimensional electron gas in a strong magnetic field, Phys. Rev. B **19**, 5211 (1979).

[34] D. Yoshioka and H. Fukuyama, Charge density wave state of two-dimensional electrons in strong magnetic fields, J. Phys. Soc. Jpn. **47**, 394 (1979).

[35] D. Yoshioka and P. A. Lee, Ground-state energy of a two-dimensional charge-density-wave state in a strong magnetic field, Phys. Rev. B **27**, 4986 (1983).

[36] R. Tao and D. J. Thouless, Fractional quantization of Hall conductance, Phys. Rev. B **28**, 1142 (1983).

[37] R. Tao, Fractional quantization of Hall conductance. II, Phys. Rev. B **29**, 636 (1984).

[38] R. Haussmann, Electronic spectral function for a two-dimensional electron system in the fractional quantum Hall regime, Phys. Rev. B **53**, 7357 (1996).

[39] R. C. Ashoori, J. A. Lebens, N. P. Bigelow, and R. H. Silsbee, Equilibrium tunneling from the two-dimensional electron gas in GaAs: Evidence for a magnetic-field-induced energy gap, Phys. Rev. Lett. **64**, 681 (1990).

[40] R. C. Ashoori, J. A. Lebens, N. P. Bigelow, and R. H. Silsbee, Energy gaps of the two-dimensional electron gas explored with equilibrium tunneling spectroscopy, Phys. Rev. B **48**, 4616 (1993).

[41] J. P. Eisenstein, L. N. Pfeiffer, and K. W. West, Coulomb barrier to tunneling between parallel two-dimensional electron systems, Phys. Rev. Lett. **69**, 3804 (1992).

[42] K. M. Brown, N. Turner, J. T. Nicholls, E. H. Linfield, M. Pepper, D. A. Ritchie, and G. A. C. Jones, Tunneling between two-dimensional electron gases in a strong magnetic field, Phys. Rev. B **50**, 15465 (1994).

[43] J. P. Eisenstein, L. N. Pfeiffer, and K. W. West, Evidence for an interlayer exciton in tunneling between two-dimensional electron systems, Phys. Rev. Lett. **74**, 1419 (1995).

[44] J. P. Eisenstein, T. Khaire, D. Nandi, A. D. K. Finck, L. N. Pfeiffer, and K. W. West, Spin and the Coulomb gap in the half-filled lowest Landau level, Phys. Rev. B **94**, 125409 (2016).

[45] A. M. Chang, M. A. Paalanen, D. C. Tsui, H. L. Störmer, and J. C. M. Hwang, Fractional quantum Hall effect at low temperatures, Phys. Rev. B **28**, 6133 (1983).

[46] L. Hedin, New method for calculating the one-particle Green's function with application to the electron-gas problem, Phys. Rev. **139**, A796 (1965).

[47] K. Van Houcke, E. Kozik, N. Prokof'ev, and B. Svistunov, Diagrammatic Monte Carlo, Phys. Proc. **6**, 95 (2010).

[48] E. Kozik, K. Van Houcke, E. Gull, L. Pollet, N. Prokof'ev, B. Svistunov, and M. Troyer, Diagrammatic Monte Carlo for correlated fermions, Europhys. Lett. **90**, 10004 (2010).

[49] K. Van Houcke, F. Werner, T. Ohgoe, N. V. Prokof'ev, and B. V. Svistunov, Diagrammatic Monte Carlo algorithm for the resonant Fermi gas, Phys. Rev. B **99**, 035140 (2019).

[50] K. Chen and K. Haule, A combined variational and diagrammatic quantum Monte Carlo approach to the many-electron problem, Nat. Commun. **10**, 3725 (2019).

[51] E. Kozik, Combinatorial summation of Feynman diagrams: Equation of state of the 2D SU(N) Hubbard model, arXiv:2309.13774.

[52] S. Sachdev and J. Ye, Gapless spin-fluid ground state in a random quantum Heisenberg magnet, Phys. Rev. Lett. **70**, 3339 (1993).

[53] A. Kitaev, A simple model of quantum holography, *Proceedings of the KITP Program: Entanglement in Strongly-Correlated Quantum Matter* (KITP, 2015).

[54] D. Chowdhury, A. Georges, O. Parcollet, and S. Sachdev, Sachdev-Ye-Kitaev models and beyond: Window into non-Fermi liquids, Rev. Mod. Phys. **94**, 035004 (2022).

[55] I. Esterlis and J. Schmalian, Cooper pairing of incoherent electrons: An electron-phonon version of the Sachdev-Ye-Kitaev model, Phys. Rev. B **100**, 115132 (2019).

[56] Y. Wang, Solvable strong-coupling quantum-dot model with a non-Fermi-liquid pairing transition, Phys. Rev. Lett. **124**, 017002 (2020).

[57] D. Hauck, M. J. Klug, I. Esterlis, and J. Schmalian, Eliashberg equations for an electron–phonon version of the Sachdev–Ye–Kitaev model: Pair breaking in non-Fermi liquid superconductors, Ann. Phys. **417**, 168120 (2020), eliashberg theory at 60: Strong-coupling superconductivity and beyond.

[58] S. Sachdev, Bekenstein-Hawking entropy and strange metals, Phys. Rev. X **5**, 041025 (2015).

[59] J. Maldacena and D. Stanford, Remarks on the Sachdev-Ye-Kitaev model, Phys. Rev. D **94**, 106002 (2016).

[60] K. Jensen, Chaos in AdS$_2$ holography, Phys. Rev. Lett. **117**, 111601 (2016).

[61] X.-Y. Song, C.-M. Jian, and L. Balents, Strongly correlated metal built from Sachdev-Ye-Kitaev models, Phys. Rev. Lett. **119**, 216601 (2017).

[62] D. Chowdhury, Y. Werman, E. Berg, and T. Senthil, Translationally invariant non-Fermi-liquid metals with critical Fermi surfaces: Solvable models, Phys. Rev. X **8**, 031024 (2018).

[63] A. A. Patel, J. McGreevy, D. P. Arovas, and S. Sachdev, Magnetotransport in a model of a disordered strange metal, Phys. Rev. X **8**, 021049 (2018).

[64] P. Cha, N. Wentzell, O. Parcollet, A. Georges, and E.-A. Kim, Linear resistivity and Sachdev-Ye-Kitaev (SYK) spin liquid behavior in a quantum critical metal with spin-1/2 fermions, Proc. Natl. Acad. Sci. USA **117**, 18341 (2020).

[65] S. Martin, A. T. Fiory, R. M. Fleming, L. F. Schneemeyer, and J. V. Waszczak, Normal-state transport properties of $Bi_{2+x}Sr_{2-y}CuO_{6+\delta}$ crystals, Phys. Rev. B **41**, 846 (1990).

[66] H. Takagi, B. Batlogg, H. L. Kao, J. Kwo, R. J. Cava, J. J. Krajewski, and W. F. Peck, Systematic evolution of temperature-dependent resistivity in $La_{2-x}Sr_xCuO_4$, Phys. Rev. Lett. **69**, 2975 (1992).

[67] T. Valla, A. V. Fedorov, P. D. Johnson, Q. Li, G. D. Gu, and N. Koshizuka, Temperature dependent scattering rates at the

Fermi surface of optimally doped $Bi_2Sr_2CaCu_2O_{8+\delta}$, Phys. Rev. Lett. **85**, 828 (2000).

[68] Y. P. Chen, G. Sambandamurthy, Z. H. Wang, R. M. Lewis, L. W. Engel, D. C. Tsui, P. D. Ye, L. N. Pfeiffer, and K. W. West, Melting of a 2D quantum electron solid in high magnetic field, Nat. Phys. **2**, 452 (2006).

[69] T. Azeyanagi, F. Ferrari, and F. I. Schaposnik Massolo, Phase diagram of planar matrix quantum mechanics, tensor, and sachdev-Ye-Kitaev models, Phys. Rev. Lett. **120**, 061602 (2018).

[70] F. Ferrari and F. I. Schaposnik Massolo, Phases of melonic quantum mechanics, Phys. Rev. D **100**, 026007 (2019).

[71] J. C. Louw and S. Kehrein, Shared universality of charged black holes and the complex large-$q$ Sachdev-Ye-Kitaev model, Phys. Rev. B **107**, 075132 (2023).

[72] R. L. Willett, H. L. Stormer, D. C. Tsui, L. N. Pfeiffer, K. W. West, and K. W. Baldwin, Termination of the series of fractional quantum Hall states at small filling factors, Phys. Rev. B **38**, 7881 (1988).

[73] H. W. Jiang, R. L. Willett, H. L. Stormer, D. C. Tsui, L. N. Pfeiffer, and K. W. West, Quantum liquid versus electron solid around $\nu=1/5$ Landau-level filling, Phys. Rev. Lett. **65**, 633 (1990).

[74] V. J. Goldman, M. Santos, M. Shayegan, and J. E. Cunningham, Evidence for two-dimentional quantum Wigner crystal, Phys. Rev. Lett. **65**, 2189 (1990).

[75] H. W. Jiang, H. L. Stormer, D. C. Tsui, L. N. Pfeiffer, and K. W. West, Magnetotransport studies of the insulating phase around $\nu=1/5$ Landau-level filling, Phys. Rev. B **44**, 8107 (1991).

[76] F. I. B. Williams, P. A. Wright, R. G. Clark, E. Y. Andrei, G. Deville, D. C. Glattli, O. Probst, B. Etienne, C. Dorin, C. T. Foxon, and J. J. Harris, Conduction threshold and pinning frequency of magnetically induced Wigner solid, Phys. Rev. Lett. **66**, 3285 (1991).

[77] M. A. Paalanen, R. L. Willett, R. R. Ruel, P. B. Littlewood, K. W. West, and L. N. Pfeiffer, Electrical conductivity and Wigner crystallization, Phys. Rev. B **45**, 13784 (1992).

[78] I. V. Kukushkin, N. J. Pulsford, K. von Klitzing, R. J. Haug, K. Ploog, and V. B. Timofeev, Wigner solid vs. incompressible laughlin liquid: Phase diagram derived from time-resolved photoluminescence, Europhys. Lett. **23**, 211 (1993).

[79] E. J. Bergholtz and A. Karlhede, Half-filled lowest landau level on a thin torus, Phys. Rev. Lett. **94**, 026802 (2005).

[80] E. J. Bergholtz and A. Karlhede, 'One-dimensional' theory of the quantum Hall system, J. Stat. Mech.: Theory Exp. (2006) L04001.

[81] E. J. Bergholtz, T. H. Hansson, M. Hermanns, and A. Karlhede, Microscopic theory of the quantum Hall hierarchy, Phys. Rev. Lett. **99**, 256803 (2007).

[82] E. J. Bergholtz and A. Karlhede, Quantum Hall system in tao-thouless limit, Phys. Rev. B **77**, 155308 (2008).

[83] Y. Cao, D. Chowdhury, D. Rodan-Legrain, O. Rubies-Bigorda, K. Watanabe, T. Taniguchi, T. Senthil, and P. Jarillo-Herrero, Strange metal in magic-angle graphene with near Planckian dissipation, Phys. Rev. Lett. **124**, 076801 (2020).

[84] R. Lyu, Z. Tuchfeld, N. Verma, H. Tian, K. Watanabe, T. Taniguchi, C. N. Lau, M. Randeria, and M. Bockrath, Strange metal behavior of the Hall angle in twisted bilayer graphene, Phys. Rev. B **103**, 245424 (2021).

[85] A. Jaoui, I. Das, G. Di Battista, J. Díez-Mérida, X. Lu, K. Watanabe, T. Taniguchi, H. Ishizuka, L. Levitov, and D. K. Efetov, Quantum critical behaviour in magic-angle twisted bilayer graphene, Nat. Phys. **18**, 633 (2022).

[86] Y. Cao, V. Fatemi, A. Demir, S. Fang, S. L. Tomarken, J. Y. Luo, J. D. Sanchez-Yamagishi, K. Watanabe, T. Taniguchi, E. Kaxiras, R. C. Ashoori, and P. Jarillo-Herrero, Correlated insulator behaviour at half-filling in magic-angle graphene superlattices, Nature (London) **556**, 80 (2018).

[87] S. Zhang, X. Lu, and J. Liu, Correlated insulators, density wave states, and their nonlinear optical response in magic-angle twisted bilayer graphene, Phys. Rev. Lett. **128**, 247402 (2022).

[88] A. Chen, R. Ilan, F. de Juan, D. I. Pikulin, and M. Franz, Quantum holography in a graphene flake with an irregular boundary, Phys. Rev. Lett. **121**, 036403 (2018).

[89] M. Brzezińska, Y. Guan, O. V. Yazyev, S. Sachdev, and A. Kruchkov, Engineering SYK interactions in disordered graphene flakes under realistic experimental conditions, Phys. Rev. Lett. **131**, 036503 (2023).

[90] A. Seidel, H. Fu, D.-H. Lee, J. M. Leinaas, and J. Moore, Incompressible quantum liquids and new conservation laws, Phys. Rev. Lett. **95**, 266405 (2005).

[91] R. Tao, A. Widom, Z. C. Tao, and H.-K. Sim, Thermodynamic Stability of the two-dimensional Jellium model in a strong magnetic field, Int. J. Mod. Phys. B **03**, 129 (1989).

[92] S. V. Kravchenko, D. A. Rinberg, S. G. Semenchinsky, and V. M. Pudalov, Evidence for the influence of electron-electron interaction on the chemical potential of the two-dimensional electron gas, Phys. Rev. B **42**, 3741 (1990).

[93] J. P. Eisenstein, L. N. Pfeiffer, and K. W. West, Negative compressibility of interacting two-dimensional electron and quasiparticle gases, Phys. Rev. Lett. **68**, 674 (1992).

[94] J. P. Eisenstein, L. N. Pfeiffer, and K. W. West, Compressibility of the two-dimensional electron gas: Measurements of the zero-field exchange energy and fractional quantum Hall gap, Phys. Rev. B **50**, 1760 (1994).

[95] R. Prange and S. Girvin, eds., *The Quantum Hall Effect*, Graduate Texts in Contemporary Physics (Springer, New York, 1989).

[96] A. Abrikosov, L. Gorkov, I. Dzyaloshinski, and R. Silverman, *Methods of Quantum Field Theory in Statistical Physics*, Dover Books on Physics (Dover Publications, New York, 2012).

[97] F. J. Dyson, Divergence of perturbation theory in quantum electrodynamics, Phys. Rev. **85**, 631 (1952).

[98] W. Wu, M. Ferrero, A. Georges, and E. Kozik, Controlling Feynman diagrammatic expansions: Physical nature of the pseudogap in the two-dimensional Hubbard model, Phys. Rev. B **96**, 041105(R) (2017).

[99] R. Rossi, F. Werner, N. Prokof'ev, and B. Svistunov, Shifted-action expansion and applicability of dressed diagrammatic schemes, Phys. Rev. B **93**, 161102(R) (2016).

[100] A. J. Kim, N. V. Prokof'ev, B. V. Svistunov, and E. Kozik, Homotopic action: A pathway to convergent diagrammatic theories, Phys. Rev. Lett. **126**, 257001 (2021).

[101] N. V. Prokof'ev and B. V. Svistunov, Polaron problem by diagrammatic quantum Monte Carlo, Phys. Rev. Lett. **81**, 2514 (1998).

[102] K. Van Houcke, F. Werner, E. Kozik, N. Prokof'ev, B. Svistunov, M. J. H. Ku, A. T. Sommer, L. W. Cheuk, A.

Schirotzek, and M. W. Zwierlein, Feynman diagrams versus Fermi-gas Feynman emulator, Nat. Phys. **8**, 366 (2012).

[103] J. Kaye, K. Chen, and O. Parcollet, Discrete Lehmann representation of imaginary time Green's functions, Phys. Rev. B **105**, 235115 (2022).

[104] H. Bruus and K. Flensberg, *Many-Body Quantum Theory in Condensed Matter Physics: An Introduction*, Oxford Graduate Texts (Oxford University Press, Oxford, 2004).

[105] M. van Schilfgaarde, T. Kotani, and S. Faleev, Quasiparticle self-consistent *GW* theory, Phys. Rev. Lett. **96**, 226402 (2006).

[106] T. Kotani, M. van Schilfgaarde, S. V. Faleev, and A. Chantis, Quasiparticle self-consistent GW method: A short summary, J. Phys.: Condens. Matter **19**, 365236 (2007).

[107] F. Hüser, T. Olsen, and K. S. Thygesen, Quasiparticle GW calculations for solids, molecules, and two-dimensional materials, Phys. Rev. B **87**, 235132 (2013).

[108] S. He, P. M. Platzman, and B. I. Halperin, Tunneling into a two-dimensional electron system in a strong magnetic field, Phys. Rev. Lett. **71**, 777 (1993).

[109] Y. B. Kim and X.-G. Wen, Instantons and the spectral function of electrons in the half-filled Landau level, Phys. Rev. B **50**, 8078 (1994).

[110] S. A. Trugman and S. Kivelson, Exact results for the fractional quantum Hall effect with general interactions, Phys. Rev. B **31**, 5280 (1985).

[111] G. Baym and L. P. Kadanoff, Conservation laws and correlation functions, Phys. Rev. **124**, 287 (1961).

[112] O. Parcollet and A. Georges, Non-Fermi-liquid regime of a doped Mott insulator, Phys. Rev. B **59**, 5341 (1999).

[113] E. G. C. P. van Loon, F. Krien, and A. A. Katanin, Bethe-Salpeter equation at the critical end point of the mott transition, Phys. Rev. Lett. **125**, 136402 (2020).

[114] E. G. C. P. van Loon, Two-particle correlations and the metal-insulator transition: Iterated perturbation theory revisited, Phys. Rev. B **105**, 245104 (2022).

[115] A. L. Efros and F. G. Pikus, Classical approach to the gap in the tunneling density of states of a two-dimensional electron liquid in a strong magnetic field, Phys. Rev. B **48**, 14694 (1993).

[116] P. Johansson and J. M. Kinaret, Magnetophonon shakeup in a Wigner crystal: Applications to tunneling spectroscopy in the quantum Hall regime, Phys. Rev. Lett. **71**, 1435 (1993).

[117] Y. Hatsugai, P.-A. Bares, and X. G. Wen, Electron spectral function of an interacting two dimensional electron gas in a strong magnetic field, Phys. Rev. Lett. **71**, 424 (1993).

[118] B. I. Halperin, Theories for $\nu = 1/2$ in single- and double-layer systems, Surf. Sci. **305**, 1 (1994).

[119] K. A. Villegas Rosales, P. T. Madathil, Y. J. Chung, L. N. Pfeiffer, K. W. West, K. W. Baldwin, and M. Shayegan, Fractional quantum Hall effect energy gaps: Role of electron layer thickness, Phys. Rev. Lett. **127**, 056801 (2021).

[120] D. Maryenko, A. McCollam, J. Falson, Y. Kozuka, J. Bruin, U. Zeitler, and M. Kawasaki, Composite fermion liquid to Wigner solid transition in the lowest Landau level of zinc oxide, Nat. Commun. **9**, 4356 (2018).

[121] G. Rohringer, H. Hafermann, A. Toschi, A. A. Katanin, A. E. Antipov, M. I. Katsnelson, A. I. Lichtenstein, A. N. Rubtsov, and K. Held, Diagrammatic routes to nonlocal correlations beyond dynamical mean field theory, Rev. Mod. Phys. **90**, 025003 (2018).

[122] G. F. Giuliani and J. J. Quinn, Breakdown of the random-phase approximation in the fractional-quantum-Hall-effect regime, Phys. Rev. B **31**, 3451 (1985).

[123] D. J. Thouless, Long-range order and the fractional quantum Hall effect, Phys. Rev. B **31**, 8305 (1985).